SUPPORTING INFORMATION

Preparation and practical applications of 2',7'-dichlorodihydrofluorescein in redox assays

Megan J. Reiniers[1,2], Rowan F. van Golen[1], Sylvestre Bonnet[3], Mans Broekgaarden[1], Thomas M. van Gulik[1], Maarten R. Egmond[2], Michal Heger[1,2]*

[1] *Department of Experimental Surgery, Academic Medical Center, University of Amsterdam, Amsterdam, the Netherlands*

[2] *Membrane Biochemistry and Biophysics, Institute of Biomembranes, Utrecht University, Utrecht, the Netherlands*

[3] *Leiden Institute of Chemistry, Leiden University, Leiden, the Netherlands*

*Corresponding author:
Michal Heger
Department of Experimental Surgery
Academic Medical Center
University of Amsterdam
Meibergdreef 9
1105 AZ Amsterdam
The Netherlands
Tel: +31 20 5665573
Fax: +31 20 6976621
Email: m.heger@amc.uva.nl

Table of contents

List of abbreviations

ACS	American Chemical Society
AlPC	aluminum phthalocyanine
APC	allophycocyanin
AUC	area under the curve
BSA	bovine serum albumin
CDCF	5(6)-carboxy-2',7'-dichlorofluorescein
DCF	2',7'-dichlorofluorescein
$DCFH_2$	2',7'-dichlorodihydrofluorescein
$DCFH_2$-DA	2',7'-dichlorodihydrofluorescein diacetate
DMEM	Dulbecco's modified Eagle medium
DMSO	dimethyl sulfoxide
DPI	diphenyleneiodonium
DPPC	1,2-dipalmitoyl-*sn*-glycero-3-phosphocholine
DSPC	1,2-distearoyl-*sn*-glycero-3-phosphocholine
$DSPE\text{-}PEG_{2000}$	1,2-distearoyl-*sn*-glycero-3-phosphoethanolamine-*N*-[methoxypolyethylene glycol-2000]
ESI-MS	electrospray ionization mass spectrometry
EtOH	ethanol
FACS	fluorescence-assisted cell sorting
FBS	fetal bovine serum
FSC	forward-scattered light
GM1	galactose-bearing ganglioside GM1
HCl	hydrochloric acid
IFN-γ	interferon gamma
IR	ischemia/reperfusion
KC	Kupffer cell
L-NAME	*N*ω-nitro-L-arginine methyl ester hydrochloride
LPE	1,2-dioleoyl-*sn*-glycero-3-phosphoethanolamine-*N*-lactosyl
MeOH	methanol
NBD-PC	1-palmitoyl-2-{12-[(7-nitro-2-1,3-benzoxadiazol-4-yl)amino]dodecanoyl}-*sn*-glycero-3-phosphocholine
NMR	nuclear magnetic resonance
NOX2	NADPH oxidase-2
PBS	phosphate-buffered saline
PGE1	prostaglandin E1
PMA	phorbol 12-myristate 13-acetate
PMT	photomultiplier tube
ppm	parts per million
PRP	platelet-rich plasma
PS	photosensitizer
R_f	retardation factor
RNS	reactive nitrogen species
ROS	reactive oxygen species
RT	room temperature
SSC	side-scattered light
SOP	standard operating procedure
TLC	thin layer chromatography
TM	transition metal

UV	ultraviolet
WE	William's E
WST-1	water soluble tetrazolium salt-1
ZnPC	zinc phthalocyanine

S–I. Chemicals, reagents, and instruments

A list of all the chemicals and reagents used in this study is provided in Table S1.

Table S1. List of chemicals and reagents.

Compound	Purity	Supplier	Additional information
18:1 lactosyl PE	> 99%	Avanti Polar Lipids[$]	Dissolved in $CHCl_3$, stored under N_2 at -20°C
AlPC	~ 85%	Sigma-Aldrich[#]	
DPPC	> 99%	Avanti Polar Lipids[$]	Dissolved in $CHCl_3$
DSPC	> 99%	Avanti Polar Lipids[$]	Dissolved in $CHCl_3$
DSPE-PEG_{2000}	n/a	Sigma-Aldrich[#]	Dissolved in $CHCl_3$
16:0-12:0 NBD PC	> 99%	Avanti Polar Lipids[$]	Dissolved in $CHCl_3$, stored under N_2 at -20°C
DCF	~ 90%	Sigma-Aldrich[#]	
$DCFH_2$-DA	≥ 90%	Molecular Probes via Thermo Scientific[¥]	Dissolved in DMSO, stored under N_2 at -20°C
Accutase	n/a	Sigma-Aldrich[#]	
Accumax	n/a	Sigma-Aldrich[#]	
APC anti-mouse CD146	n/a	BioLegend[‡]	Clone ME-9F1
α-Lipoic acid	≥ 99%	Sigma-Aldrich[#]	
α-Tocopherol	≥ 96%	Sigma-Aldrich[#]	1 mM in $CHCl_3$
Bovine serum albumin	≥ 98%	Sigma-Aldrich[#]	
Brilliant Violet 421 anti-mouse F4/80	n/a	BioLegend[‡]	Clone BM8
$CaCl_2 \cdot 2\ H_2O$	≥ 99.9%	Merck Millipore*	
$CHCl_3$	≥ 99%	Sigma-Aldrich[#]	
Cholesterol	> 98%	Avanti Polar Lipids[$]	Dissolved in $CHCl_3$, stored under N_2 at -20°C
Citric acid	≥ 99.5%	Sigma-Aldrich[#]	
Collagenase IV	≥125 CDU/mg	Sigma-Aldrich[#]	
Convulxin	n/a	Kordia[§]	10 µg/mL in MilliQ
CuCl	≥ 99.995%	Sigma-Aldrich[#]	300 mM in 2.5 M NaCl in MilliQ
Curcumin	≥ 95%	Fluka[¶]	Dissolved in ethanol, shielded from light
D(+)-glucose	≥ 99.8%	Merck Millipore*	
Diphenyleneiodonium	≥ 98%	Sigma-Aldrich[#]	625 µM in DMSO
DMSO	≥ 99.5%	Merck Millipore*	
DMSO-d6	99.96 atom% d	Sigma-Aldrich[#]	
Dulbecco's modified Eagle medium	n/a	Lonza[†]	
$Fe(II)Cl_2$	99.998%	Sigma-Aldrich[#]	300 mM in EtOH
$Fe(II)SO_4$ (heptahydrate)	≥ 99%	Sigma-Aldrich[#]	30 mM in MilliQ, pH = 1, prepared freshly before each experiment
FBS	n/a	Bodinco[@]	
Fish sperm DNA	≤ 1% protein	Sigma-Aldrich[#]	$Abs_{260/280\ nm} \geq 1.5$
γ-Tocopherol	≥ 96%	Sigma-Aldrich[#]	
Ganglioside GM1	> 99%	Avanti Polar Lipids[$]	Dissolved in $CHCl_3$:CH_3OH:H_2O [65:35:8, v/v], stored under N_2
HCl	37%	Sigma-Aldrich[#]	
H_2O_2 (30%)	n/a	Merck Millipore*	
HEPES	≥ 99%	Merck Millipore*	
HEPES (sodium salt)	≥ 99.5%	Sigma-Aldrich[#]	

Hoechst 33342	> 95%	Thermo Scientific[¥]	
Human recombinant insulin solution	≥ 27 U/mg	Sigma-Aldrich[#]	
Hydrocortisone 21-hemisuccinate	n/a	Sigma-Aldrich[#]	
Isoflurane	n/a	Abbott Laboratories[€]	
KCl	≥ 99%	Sigma-Aldrich[#]	
KH_2PO_4	≥ 99%	Merck Millipore*	
L-glutamine	n/a	Lonza[†]	
Melatonin	≥ 98%	Sigma-Aldrich[#]	
MeOH	≥ 99.9%	Sigma-Aldrich[#]	
MeOH-d4	99.96 atom% d	Sigma-Aldrich[#]	
$MgCl_2 \cdot 8\ H_2O$	≥ 99.9%	Merck Millipore*	
$MnCl_2$	99.999%	Sigma-Aldrich[#]	1 M in EtOH
Mouse recombinant IFN-γ	≥ $1.0 \cdot 10^7$ U/mg	Merck Millipore*	Reconstituted in phosphate buffer (10 mM Na_2HPO_4, 0.1% BSA, pH = 8.0)
L-NAME	≥ 98%	Sigma-Aldrich[#]	90 mM in PBS
Trisodium citrate • 2 H_2O	≥ 99%	Sigma-Aldrich[#]	
NaCl	≥ 99%	Sigma-Aldrich[#]	
$NaHCO_3$	≥ 99%	Merck Millipore*	
$Na_2HPO_4 \cdot 2\ H_2O$	≥ 99%	Merck Millipore*	
$NaH_2PO_4 \cdot 2\ H_2O$	≥ 99%	Merck Millipore*	
NaOH	≥ 97%	Sigma-Aldrich[#]	
Paraformaldehyde	n/a	Merck Millipore*	
Penicillin/streptomycin	n/a	Lonza[†]	
PMA	≥ 99%	Sigma-Aldrich[#]	2 mM in DMSO
Prostaglandin E_1	≥ 98%	Sigma-Aldrich[#]	
Temgesic (buprenorphine)	n/a	Schering-Plough[&]	
Tetramethylsilane	≥ 99.99%	Sigma-Aldrich[#]	
Thrombin from human plasma	≥ 2800 U/mg	Sigma-Aldrich[#]	125 U/mL in MilliQ
Triton X-100	≥ 99.95%	Sigma-Aldrich[#]	
William's E medium	n/a	Lonza[†]	Without phenol red
WST-1 cell proliferation reagent	n/a	Roche via Sigma-Aldrich[#]	
$ZnCl_2$	99.999%	Sigma-Aldrich[#]	3 M in EtOH
ZnPC	97%	Sigma-Aldrich[#]	

* Darmstadt, Germany
[#] St. Louis, MO
[†] Basel, Switzerland
[¶] Buchs, Switzerland
[$] Alabaster, AL
[¥] Rockford, IL
[§] Kordia l Stago, Leiden, the Netherlands
[‡] San Diego, CA
[&] Kenilworth, NJ
[€] Queensborough, UK
[@] Alkmaar, the Netherlands

$DCFH_2$-DA was dissolved in dimethylsulfoxide (DMSO) or methanol (MeOH) up to a 50-mM concentration, respectively, and stored in aliquots under N_2 gas at -20 ºC in the dark. DCF was dissolved in MeOH and stored at room temperature (RT) in the dark. All other reagents are detailed in Table S1. The concentrations listed throughout the manuscript refer to final concentrations unless stated otherwise.

UV/VIS absorption spectroscopy (Lambda 18, Perkin Elmer, Waltham, MA) was performed at 120-nm/min scan speed and 0.5-nm bandwidth. Fluorescence spectroscopy (Varian Cary Eclipse, Palo Alto, CA) was performed at 120-nm/min scan speed. Absorption and fluorescence spectroscopy

were performed using 1-cm path length quartz cuvettes (Hellma Analytics, Müllheim, Germany). *In vitro* fluorescence spectroscopy was performed in a microplate reader (Synergy HT, BioTek Instruments, Winooski, VT) and flow cytometry with a FACSCanto II system (Becton Dickinson, Franklin Lakes, NJ).

^{1}H and ^{13}C nuclear magnetic resonance (NMR) spectra were recorded with a DPX 300 and DMX 400 spectrometer, respectively (Bruker, Billerica, MA). The chemical shifts are given in ppm relative to tetramethylsilane. Electrospray ionization mass spectrometry (ESI-MS; Finnigan TSQ Quantum, Thermo Electron, San Jose, CA) was performed in negative ion mode.

PART 1: PREPARATION AND CHARACTERIZATION OF $DCFH_2$

S–II. Determination of optimal NaOH concentration for the $DCFH_2$-DA → $DCFH_2$ deacetylation reaction

$DCFH_2$ was prepared from $DCFH_2$-DA by deacetylation under alkaline conditions. To determine the optimal reaction conditions in terms of NaOH concentration, the deacetylation of $DCFH_2$-DA was studied at increasing NaOH concentrations by absorption spectroscopy.

Materials and methods: Absorption spectroscopy was performed in kinetics mode, in which $DCFH_2$-DA in DMSO was added to a cuvette (20 µM $DCFH_2$-DA, 0.4% DMSO) containing increasing concentrations of NaOH (0-5 M in MilliQ) during continuous magnetic stirring. Absorption was determined at 30-s intervals at λ = 265 nm (near absorption maximum of $DCFH_2$-DA), 300 nm (near absorption maximum of $DCFH_2$), and 500 nm (near absorption maximum of DCF). The assays at λ = 500 nm were conducted to determine whether $DCFH_2$ auto-oxidizes to DCF in alkaline solution. In addition, absorption spectra were recorded (λ = 200-400 nm) following incubation of $DCFH_2$-DA (20 µM) in 0–5 M of NaOH for 20 min.

Results: An NaOH concentration-dependent decrease in absorbance was observed at 265 nm, indicating deacetylation of $DCFH_2$-DA (λ_{max} = 258 nm in MilliQ, Figure S1A, grey line). The decrease in absorbance at 265 nm concurred with an increase in absorbance at λ = 300 nm when $DCFH_2$-DA was incubated with 5 mM–1 M NaOH (Figure S1B), indicating the formation of $DCFH_2$ (λ_{max} = 305 nm at pH = 12[1]). The lower extent of $DCFH_2$ formation observed for the 5-M NaOH samples likely resulted from base-catalyzed modification of $DCFH_2$, particularly since no DCF (λ_{max} = 500 nm in MilliQ[2]) was detected in the samples (Figure S1C) and thus any base-mediated $DCFH_2$ oxidation could be ruled out. Spectrally, a shift in maximum absorbance from 258 nm to 305 nm was observed after $DCFH_2$-DA deacetylation (Figure S1D, arrow), a finding that was in accordance with earlier data on the spectral properties of $DCFH_2$[1].

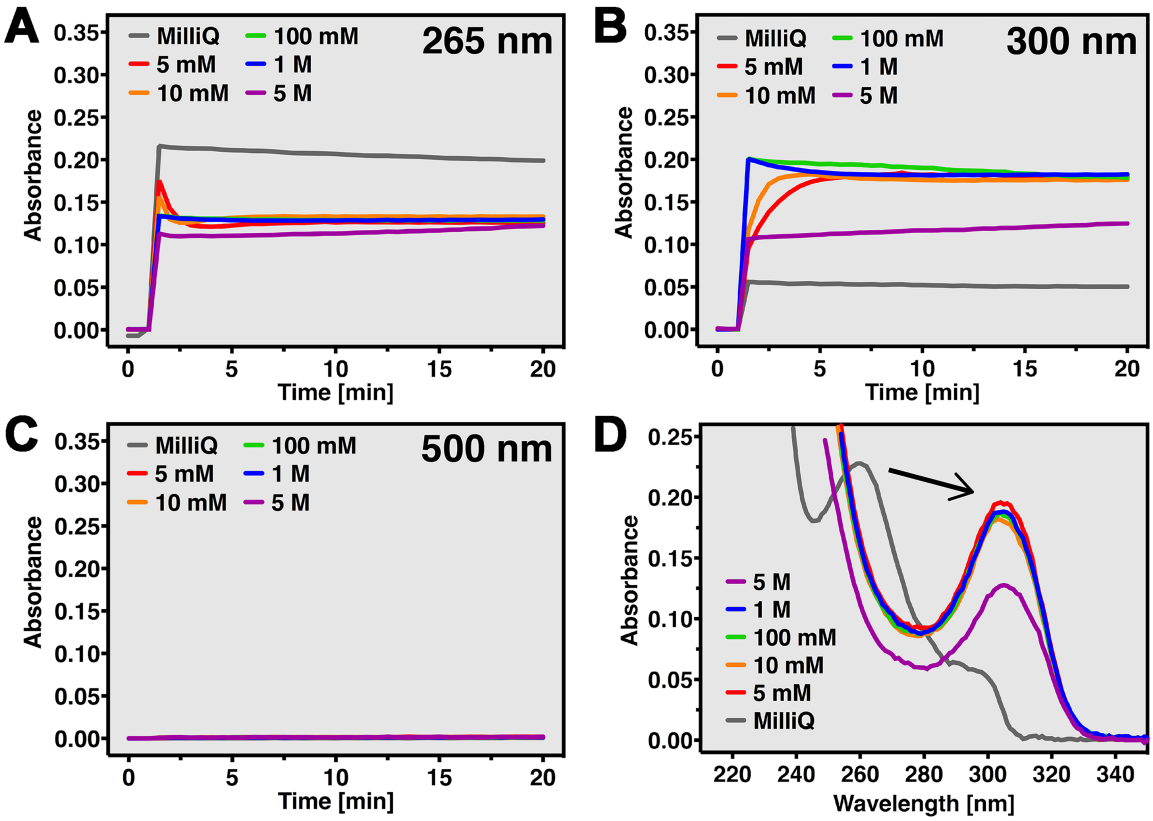

Figure S1. Time-based absorption spectroscopy (t = 20 min) of 20 µM $DCFH_2$-DA in 0-5 M NaOH at λ = 265 nm (Panel A), corresponding to the $DCFH_2$-DA absorption peak, λ = 300 nm (Panel B), corresponding to the $DCFH_2$ absorption peak, and λ = 500 nm (Panel C), corresponding to the DCF absorption peak. $DCFH_2$-DA was added to the cuvette at t = 1 min. Panel D shows absorption spectra obtained following 20-min incubation of 20 µM $DCFH_2$-DA in 0, 0.005, 0.01, 0.1, 1, or 5 M NaOH. The arrow points to the main absorption band of $DCFH_2$, which arises at the expense of the deeper UV band of $DCFH_2$-DA.

Conclusions: The deacetylation reaction proceeds optimally in 10 mM – 1 M NaOH. Increasing the NaOH concentration beyond 1 M has no added value with respect to $DCFH_2$ formation from $DCFH_2$-DA since very high base concentrations are detrimental for $DCFH_2$ yield and product purity.

S–III. Determination of $DCFH_2$ and by-product formation during alkaline hydrolysis of $DCFH_2$-DA

The end products of alkaline hydrolysis were assayed by thin layer chromatography (TLC) to assess the completeness of the $DCFH_2$-DA deacetylation reaction as a function of NaOH concentration and to determine whether $DCFH_2$ and any by-products had formed.

Materials and methods: For these purposes, 10 µL of 50 mM $DCFH_2$-DA in DMSO was incubated with 240 µL of NaOH (0.01, 0.1, 1, or 5 M) in MilliQ for 15 min at RT in the dark. Subsequently, 1.5 µL of the incubated sample was loaded on a TLC plate, together with a $DCFH_2$-DA (5 mM in DMSO, 1 µL loading volume) and DCF reference (0.5 mM in MeOH, 1 µL loading volume). TLC was performed using fluorescent plates (silica 60 F_{254} RP-8 5 × 10 cm, Merck Chemicals, Darmstadt, Germany) and a mobile phase composed of MeOH:MilliQ:$CHCl_3$:NaOH (8 M in MilliQ) at a 7:3:1:0.044 volume ratio. The loading and running were performed in a dark room. The plates were visualized in a blot imager (ECL ChemoCam Imager, INTAS Science Imaging Instruments, Göttingen, Germany) with blue light emission to allow for the detection of DCF (λ_{em} = 460 ± 40 nm). A separate UV excitation light source (λ_{ex} = 254 ± 2 nm, Mineralight, UVP, Upland, CA) was placed in the imager to visualize the TLC plates. UV light-absorbing compounds adsorbed to the silica quench the UV fluorescence emission of the silica matrix, therefore appearing as dark spots.

Results: As shown in Figure S2, a single, non-fluorescent band (retardation factor [Rf] of ~ 0.3), corresponding to that of the $DCFH_2$-DA reference sample, was visible for the sample incubated with 0 M NaOH, indicating that no deacetylation had occurred. The same band, albeit less dense, was observed for the sample incubated with 0.01 M NaOH. At the 0.01-M NaOH concentration, a second band appeared at $R_f \approx 0.50$ that comprises a reaction intermediate, possibly $DCFH_2$ monoacetate. Also, a faint third band ($R_f \approx 0.62$) was visible, corresponding to $DCFH_2$. The third band became more pronounced in the $DCFH_2$-DA samples hydrolyzed in solution containing 0.1–5 M NaOH, which coincided with the disappearance of the first 2 bands, indicating complete $DCFH_2$ → DCF conversion.

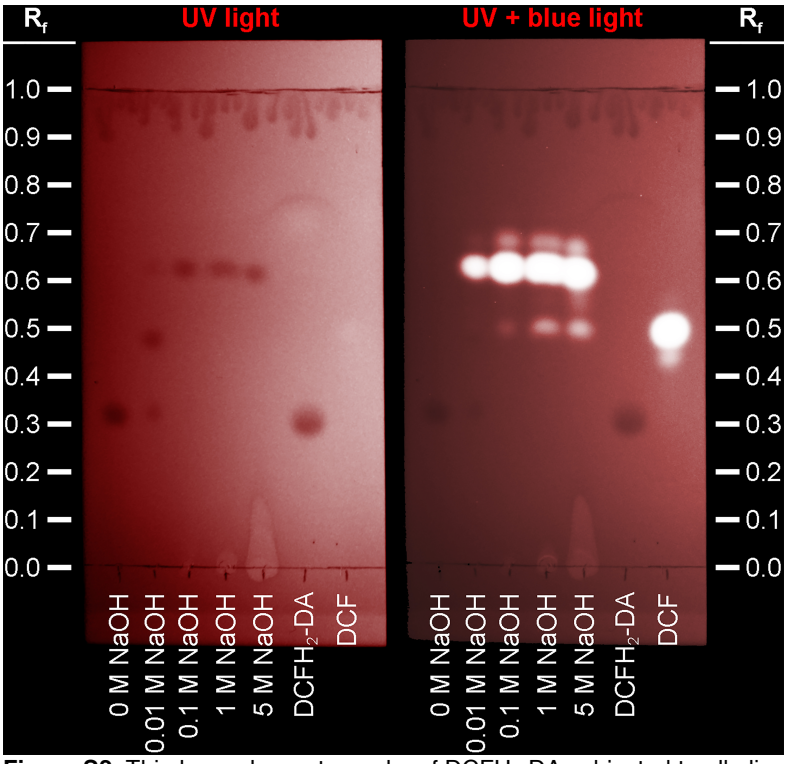

Figure S2. Thin layer chromatography of $DCFH_2$-DA subjected to alkaline hydrolysis at increasing NaOH concentrations and the untreated analytical standards $DCFH_2$-DA ($DCFH_2$ precursor) and DCF ($DCFH_2$ oxidation product). The TLC plates were visualized under UV light irradiation (left) and UV + blue light irradiation (right). R_f: retardation factor. The solvent front is at $R_f = 1.0$.

At the higher NaOH concentrations (> 0.01 M), a small amount of impurity was detected. Deacetylation with 0.1–5 M NaOH also gave rise to 2 discernible fluorescent bands under UV/blue light illumination. The lower fluorescent band ($R_f \approx 0.50$) corresponded to DCF and suggests $DCFH_2$ auto-oxidation during the experimental procedure since there is no spectroscopic evidence for DCF formation during $DCFH_2$-DA deacetylation (Figure S1D). Consequently, this phenomenon is technical in nature and associated with the TLC/solvent system and therefore of no practical concern.

The upper fluorescent band ($R_f \approx 0.68$) most likely constitutes an unknown by-product or a structurally distinct isoform of $DCFH_2$ that was separated from the main $DCFH_2$ band as a result of the deacetylation procedure. This is supported by the fact that the fluorescence intensity of that band is proportional to the amount of $DCFH_2$ formed (e.g., 0.01 M versus 0.1 M NaOH). The impurity at $R_f \approx 0.68$ is further addressed in S–V and S–VI.

Conclusions: The $DCFH_2$-DA deacetylation procedure is incomplete in solution containing < 100 mM NaOH in a 1:24 $DCFH_2$-DA stock:solvent ratio, whereas the procedure yields no additional gain in basic solutions containing > 100 mM NaOH. Furthermore, deacetylation with 100 mM NaOH yields the highest amount of $DCFH_2$ with the least amount of impurities. Consequently, $DCFH_2$-DA deacetylation in 100 mM NaOH was adopted into the standard operating procedure (SOP), i.e., 1:24 $DCFH_2$-DA:solvent ratio (v/v), 50 mM starting $DCFH_2$-DA concentration, 15-min incubation in 100 mM NaOH at RT (S–VIII).

S–IV. Purification of $DCFH_2$ and determination of product yield

Following $DCFH_2$-DA deacetylation, $DCFH_2$ was purified by liquid phase extraction and the yield was determined. The yield reflects the reaction and purification efficacy.

Materials and methods: For these purposes, 4 samples of 5 µmol $DCFH_2$-DA in MeOH (100 µL) were prepared in 2.5 mL of 0.1 M aqueous NaOH in glass tubes and incubated for 15 min at RT in the dark (SOP, S–VIII). Next, 2.5 mL of 0.2 M aqueous HCl was gradually added under continuous vortexing to precipitate $DCFH_2$. The mixture was placed on ice for 5 min to complete $DCFH_2$ precipitation, which was subsequently washed thrice (15 min, 2,000 × g, 4 °C) in ice-cold acidified MilliQ (pH = 1, from HCl) to remove excess salt. The sample was subsequently equilibrated to RT and 4 mL of $CHCl_3$ was added under continuous vortexing to extract $DCFH_2$ from the aqueous phase. Following phase separation, the aqueous phase was removed using a pipette and all $CHCl_3$ was evaporated under a continuous stream of N_2 gas at RT. $DCFH_2$ was resuspended in MeOH and samples were pooled.

Pooled $DCFH_2$ samples (n = 3) were transferred to pre-weighed 0.5-mL Eppendorf tubes, after which the MeOH was evaporated under a gentle stream of N_2 gas in the dark. The tubes were weighed again to determine the mass of the $DCFH_2$ pellet, which was used to calculate the overall $DCFH_2$ yield.

Results: Of the 20 µmol $DCFH_2$-DA added, 10.8 ± 1.2 µmol $DCFH_2$ (mean ± SEM) was retrieved, accounting for a mean (± SEM) $DCFH_2$ yield of 54.2 ± 5.8%.

Conclusions: The deacetylation and purification method, which in total takes approximately 2 h, is associated with moderate $DCFH_2$ yield whereby approximately half of the starting product ($DCFH_2$-DA) is retrieved in the form of $DCFH_2$.

S–V. Chemical characterization and purity of $DCFH_2$ by NMR and ESI-MS

The purity of purified $DCFH_2$ was first analyzed by NMR and ESI-MS. $DCFH_2$-DA and DCF were co-analyzed.

Materials and methods: $DCFH_2$-DA was dissolved in DMSO-d6 and DMSO at a concentration of 12 mg/mL and 24 mg/mL, respectively. ^{1}H NMR (400 MHz, DMSO-d6) δ 7.88 (d, 1 H), 7.49, (t, 1 H), 7.36 (t, 1 H), 7.27 (s, 2 H), 7.19 (s, 2 H), 7.07 (d, 1 H) 6.40 (s, 1 H), 2.32 (s, 6 H). ^{13}C NMR (75 MHz, DMSO-d6) δ 169.00, 168.15, 148.92, 145.93, 145.38, 132.83, 131.26, 130.16, 130.08, 129.88, 127.29, 123.22, 120.53, 112.50, 37.42, 20.38. ESI-MS m/z (calc): 485.0 (485.02, $C_{24}H_{15}Cl_2O_7^-$), 973.0 (973.04, $C_{48}H_{31}Cl_4O_{14}^-$).

$DCFH_2$ (prepared as described in S-VIII) was dissolved at 7 mg/mL in CD_3OD and MeOH for NMR spectroscopy and ESI-MS, respectively. ^{1}H NMR (400 MHz, CD_3OD) δ 7.89 (s), 7.87 (dd, 1 H), 7.39 (td, 1 H), 7.25 (td, 1 H), 6.98 (dd, 1 H), 6.92 (s, 2 H), 6.64 (s, 2 H), 6.21 (s, 1 H). ^{13}C NMR (75 MHz, CD_3OD) δ 171.51, 153.89, 151.16, 149.06, 133.48, 132.24, 131.31, 130.82, 127.52, 118.01, 116.73, 104.89, 38.25. ESI-MS m/z (calc): 401.0 (401.00, $C_{20}H_{11}Cl_2O_5^-$), 805.0 (805.00, $C_{40}H_{23}Cl_4O_{10}^-$), 827.0 (826.98, $C_{40}H_{22}Cl_4NaO_{10}^-$).

DCF was dissolved at 4 mg/mL in DMSO-d6 and 10 mg/mL in DMSO for NMR spectroscopy and ESI-MS, respectively. ^{1}H NMR (400 MHz, DMSO-d6) δ 11.09 (br s, 2 H), 8.02 (d, 1H), 7.83 (td, 1H), 7.75 (td, 1H), 7.34 (d, 1H), 6.91 (s, 2H), 6.66 (s, 2H). ^{13}C NMR (100 MHz, DMSO-d6) δ 168.29, 155.13, 151.51, 150.08, 135.92, 130.54, 128.21, 125.90, 125.10, 123.96, 116.24, 110.46, 103.70, 81.49. ESI-MS m/z (calc): 399.0 (398.98, $C_{20}H_9Cl_2O_5^-$).

Results: The ESI-MS spectrum (negative ion mode) of $DCFH_2$-DA showed the characteristic peak of the monoanion at m/z = 485.0 and its protonated dimer at m/z = 973.0. Meanwhile, $DCFH_2$ and DCF could clearly be distinguished from each other, as the first peak of the isotopic pattern was 401.0 for $DCFH_2$ and 399.0 for DCF. Next to DCF the peak at 536.8 represented the only observable impurity, which would fit with a solvent adduct of DCF ([DCF+DMSO+CH_3CN+NH_4], calc m/z = 536.1).

The 1H and 13C NMR spectra of $DCFH_2$-DA and DCF were measured in DMSO-d6, and those of $DCFH_2$ were measured in CD_3OD. The NMR spectra showed that the samples were NMR-pure and consistent with the ones reported by[3]. No sign of the acetyl groups in the acetylated form

$DCFH_2$-DA (e.g., singlet at 2.3 ppm) was found in $DCFH_2$. The lactone form of DCF (Figure S3) was obtained, characterized by a high-field chemical shift at 81.5 ppm of the quaternary carbon connected to the lactone oxygen. Importantly, the impurity seen by TLC was not observed by NMR, which means that this impurity represents less than 3–5% of the sample (detection limit for ^{1}H NMR).

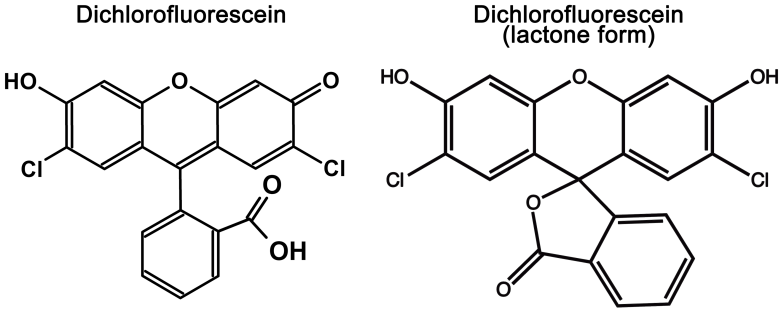

Figure S3. Molecular structure of DCF (left) compared to its lactone isomer (right).

Conclusions: Purified $DCFH_2$ was NMR pure and structurally consistent with previously reported data.

S–VI. Analysis of TLC bands by fluorescence spectroscopy

The fluorescent bands on the TLC plate were analyzed by fluorescence spectroscopy to determine the spectral properties of the fluorophores.

Thin layer chromatography

Materials and methods: TLC was performed as described in S–III under optimized conditions using purified $DCFH_2$ (5 mM in MeOH, 3 µL loading volume) that had been prepared from $DCFH_2$-DA according to the SOP (S–III). $DCFH_2$-DA (5 mM in DMSO, 1 µL loading volume) and DCF (476 µM in MeOH, 1 µL loading volume) were co-loaded as reference samples.

Results: The TLC plate was visualized by UV light only as well as by a combination of UV and blue light, yielding the same results (Figure S4) as previously (Figure S2). In UV only mode, a single band was observed for $DCFH_2$. Under UV/blue light illumination, 2 of the 3 lower bands ($R_f < 0.62$) corresponded to DCF and probably resulted from $DCFH_2$ auto-oxidation during the experimental procedure. The third, lowest band ($Rf \approx 0.43$) was very faint and was therefore considered an insignificant but unidentified by product that is structurally related to DCF.

The upper band ($R_f \approx 0.68$) most likely represents an artifact from the deacetylation procedure. Considering that this compound did not show on the NMR spectrum of $DCFH_2$ (S–V), however, it is likely to represent less than 1–5 % of the sample (i.e., the detection limit for ^{1}H NMR).

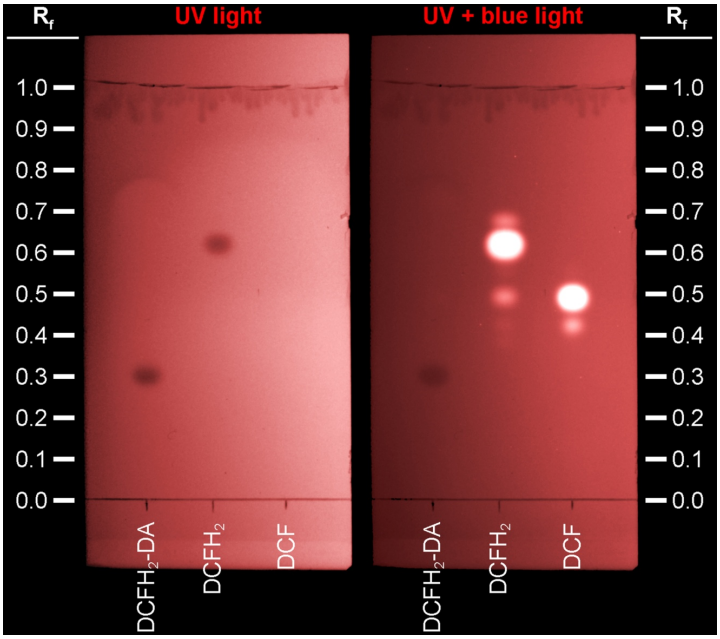

Figure S4. Thin layer chromatography of $DCFH_2$-DA, $DCFH_2$ (prepared under optimized reaction conditions), and DCF. The fluorescent bands were isolated and analyzed spectrofluorometrically.

In order to obtain additional information on the nature of the by-products, all bands (except for the lowest one because of its low intensity) from the $DCFH_2$ and DCF sample were isolated and analyzed spectrofluorometrically.

Fluorescence emission spectra of $DCFH_2$ and DCF bands

Materials and methods: Following TLC, specific $DCFH_2$ and DCF bands (Figure S4) were extracted by scraping and suspended in MeOH. The silica particles were separated by centrifugation (15 min at 6,000 × g), after which the supernatant was aspirated and analyzed spectrofluorometrically (specific details are provided in the respective Results sections). Fluorescence excitation and emission spectra were normalized to the maximum fluorescence intensity inasmuch as structural differences are mainly revealed through band shape and peak position shifts rather than amplitude differences.

Results: Fluorescence emission spectra (λ_{ex} = 480 ± 20 and λ_{em} = 505–750 ± 5 nm) of all DCF(H_2) samples were recorded together with a DCF reference sample (grey line) (Figure S5). Notably distinct emission spectra were observed in samples 1 and 2, indicating the presence of a structurally different $DCFH_2$ derivative (sample 1) and possibly the product of UV light-induced oxidized $DCFH_2$ (sample 2) that had undergone photochemical modification and hence structurally and spectrally differed from DCF. The fluorescence intensity of these samples was very low due to their low abundance, as evidenced by the 'noisy' spectra. The spectra had to be acquired at high PMT voltage at the expense of a good signal:noise ratio. All other samples corresponded well to the DCF reference sample.

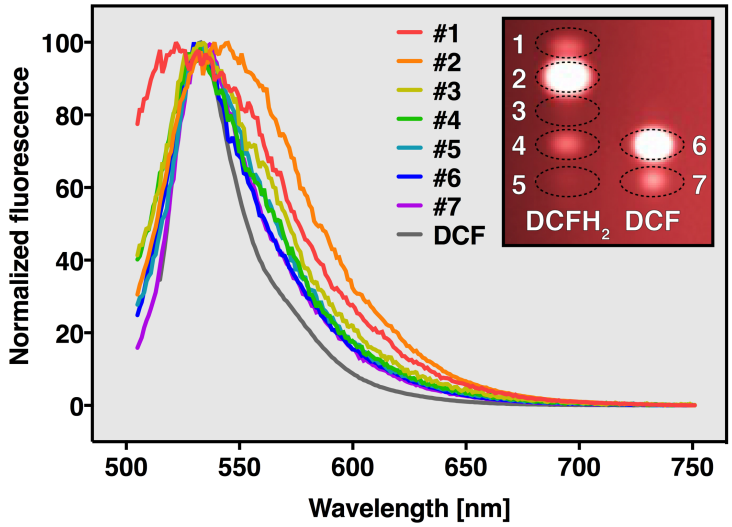

Figure S5. Fluorescence emission spectra of $DCFH_2$ and DCF TLC bands, acquired at λ_{ex} = 480 ± 20 nm and λ_{em} = 505–750 ± 5 nm. Band 1, $R_f \approx 0.68$; band 2 ($DCFH_2$), $R_f \approx 0.62$; band 3, $R_f \approx 0.56$; band 4, $R_f \approx 0.50$; band 5, $R_f \approx 0.43$; band 6 (DCF), $R_f \approx 0.50$; band 7, $R_f \approx 0.43$. A DCF reference sample was also recorded (grey trace).

Fluorescence excitation spectra of $DCFH_2$ and DCF bands

Materials and methods: Same as above, with the exception that the excitation spectra were recorded at λ_{ex} = 200–540 ± 5 and λ_{em} = 550 ± 5 nm.

Results: In accordance with the emission spectra, notable deviations from the DCF reference sample were seen for bands 1 and 2 (Figure S6). In regard to band 1, the excitation spectrum exhibited a second excitation peak around 490 nm in addition to the 515-nm peak and a more pronounced blue shoulder, indicating the formation of a structurally distinct compound with fluorescence properties comparable to those of DCF (Figure S7). The slightly red-shifted spectrum of band 2 likely represents a structurally modified $DCFH_2$ oxidation product (S–VI, *Fluorescence emission spectra of $DCFH_2$ and DCF bands*). All other samples, including sample # 7, corresponded well to the DCF reference sample, which is in accordance with the data in Figure S5.

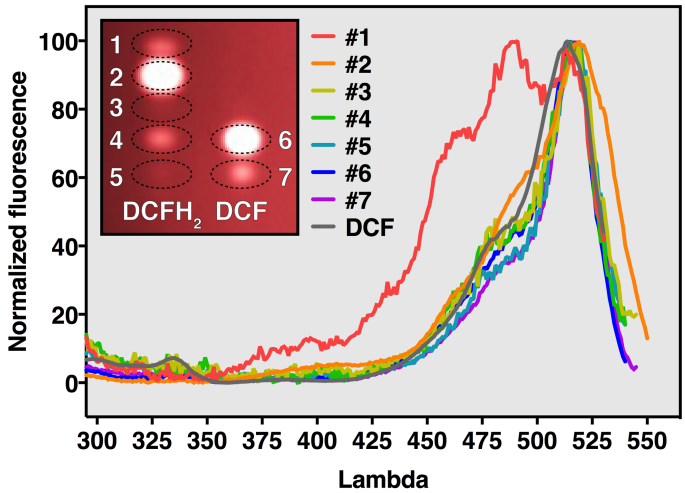

Figure S6. Fluorescence excitation spectra of $DCFH_2$ and DCF TLC bands, acquired at λ_{ex} = 200–540 ± 5 nm and λ_{em} = 550 ± 5 nm. Band 1, $R_f \approx 0.68$; band 2 ($DCFH_2$), $R_f \approx 0.62$; band 3, $R_f \approx 0.56$; band 4, $R_f \approx 0.50$; band 5, $R_f \approx 0.43$; band 6 (DCF), $R_f \approx 0.50$; band 7, $R_f \approx 0.43$. A DCF reference sample was also recorded (grey trace).

Detailed spectral analysis of $DCFH_2$-DA deacetylation-associated TLC band 1 (main impurity)

As established in S–III, the band at $R_f \approx 0.68$ constitutes an impurity that seems to arise during the deacetylation step of $DCFH_2$-DA. The impurity either stems from the parent $DCFH_2$-DA stock (≥ 95% purity) or constitutes an oxidized prototropic $DCFH_2$ tautomer that partitioned in the aqueous fraction of the TLC mobile phase. Based on the NMR spectrum of $DCFH_2$, the latter proposition was deemed more likely. Here we analyze this band in greater detail and discuss its occurrence.

Methods: Based on the acquired spectral data, the fluorescence excitation and emission properties of band 1 in MeOH were further analyzed together with the emission spectrum of DCF in MeOH (solid grey line) and the excitation spectrum of DCF in MilliQ at pH > 7 (dashed grey line) as references. At pH > 7, both the carboxylic acid and phenolic moiety on DCF are deprotonated. The spectrum was included to support the argumentation below.

Results: Two main excitation peaks were identified in the 450–550-nm range (at $\lambda_{em} = 545 \pm 5$ nm). When excited at each excitation maximum ($\lambda_{ex} = 490 \pm 5$ nm and 515 ± 5 nm), the emission spectra exhibited maxima at 521 nm and 532 nm, respectively. The latter spectrum corresponded well to the DCF spectrum ($\lambda_{max} = 533$ nm). These observations can be explained in various ways.

First, excitation spectra reflect vibronic transitions in the first excited state. Accordingly, photo-induced tautomerization may have occurred in the excited state of $DCFH_2$, accounting for a shift in spectral properties. Given that the excitation spectrum is superimposable on the excitation spectrum of DCF in MilliQ at high pH (pH > 7, $\lambda_{ex} = 490$ and 515 nm, dashed grey line), it is possible that the species accounting for the double peak is an oxidized derivative that deprotonates upon excitation; a common mechanism in for example photoacids[4]. Alternatively, the compound is a derivative species that had formed at relatively low yield during the deacetylation process but possesses a high fluorescence quantum yield.

Second, at high pH both the carboxylic acid and phenolic moiety on DCF are deprotonated ($pK_a = 3.5$ and 5.2, respectively[1,5]). The compound could therefore be fully deprotonated $DCFH_2$ ($pK_a \approx 4.00$, 6.95, and 9.17 for the carboxylic acid and two phenolic moieties, respectively[1]), which may have partitioned into the highly alkaline aqueous fraction of the TLC mobile phase and thereby become separated from other prototropic $DCFH_2$ tautomers present in the organic portion of the mobile phase (consisting of MeOH, $CHCl_3$, and a marginal fraction of highly alkaline water). Subsequent exposure to UV light during visualization could oxidize the fully deprotonated $DCFH_2$ into bi-anionic DCF, which would subsequently dissolve in MeOH (during sample preparation of the scraped bands) while maintaining its distinct spectral properties.

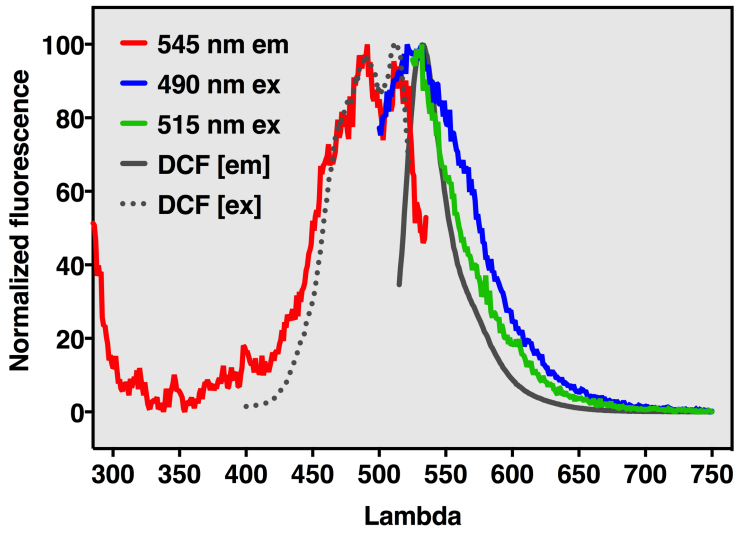

Figure S7. Fluorescence excitation and emission spectra of band 1 in the $DCFH_2$ TLC lane ($R_f \approx 0.68$) relative to the DCF reference spectra (grey). Samples were dissolved in MeOH.

Conclusions: $DCFH_2$ prepared according to this protocol and purified by liquid two-phase extraction was ≥ 95% pure. Alkaline hydrolysis of the $DCFH_2$-DA diacetate groups concurs with the formation of a fluorescent impurity with superimposable spectral properties to those of DCF. This may create background signal in $DCFH_2$-based assays. The low relative abundance of the impurity is not expected to significantly contribute to spectral signals. Moreover, the impurity will not hinder spectrofluorometric determination of oxidant formation as long as background fluorescence is corrected for.

S–VII. Residual chloride content determination

The deacetylation procedure ultimately results in high salt content due to alkalinization and subsequent acidification of the sample. The washing of precipitated $DCFH_2$ (SOP, Figure 1 main text, and S–VIII) entailed the use of MilliQ acidified with HCl. Residual chloride may hamper experimental outcomes, which is of relevance for determining $DCFH_2$ yield (S–IV) as well as for cell-based assays because cells are amenable to perturbations in osmotic gradients. Consequently, it is imperative that the prepared $DCFH_2$ samples contain no-to-minimum amount of salts. To ascertain that most Cl^- had been separated from the $DCFH_2$-containing organic phase during liquid phase extraction, the amount of Cl^- in the $CHCl_3$ fraction was determined.

Materials and methods: Cl^- content was determined using a chromometric Cl^- quantification kit (chloride colorimetric assay kit, Cayman Chemical, Ann Arbor, MI). The assay depends on the competitive binding of Hg^{2+} and Fe^{2+} to thiocyanate (SCN^-), which, in the absence of Cl^-, forms a colorless complex with Hg^{2+}. In the presence of Cl^-, however, the preferential binding of Hg^{2+} to Cl^- leads to the formation of a yellow-colored $Fe(SCN)_2$ complex that can be quantified spectrophotometrically (Abs_{max} = 480 nm) against a NaCl standard curve.

The Cl^- content in the organic phase was determined in samples (n = 10) prepared as described in S–VIII, only in the absence of $DCFH_2$. The addition of $DCFH_2$ was omitted because it is readily oxidized in the presence of Fe^{2+} to DCF[6,7]. The DCF (Abs_{max} = 503 nm)[2] would spectrally interfere with the $Fe(SCN)_2$ complex[8]. Following isolation of the organic fraction and evaporation of $CHCl_3$, 110 µL of MilliQ was added to the glass tube and the Cl^- content was determined against a 0–2,000-µM NaCl standard curve in MilliQ according to the manufacturer's instructions.

Results: The mean ± SD Cl^- content was 0.384 ± 0.122 µg per 110 µL resuspension volume (3.5 ± 1.1 µg/mL), corresponding to 140.6 ± 44.7 µg/g $DCFH_2$ (0.014% w/w, based on the calculated $DCFH_2$ yield from 5 µmol $DCFH_2$-DA).

Conclusions: The amount of residual Cl^- did not significantly contribute to the mass of $DCFH_2$, validating the data regarding yield and molar extinction coefficient. Given that $DCFH_2$ is added to samples at a very low volume ratio, the amount of residual Cl^- will not interfere with experiments and assays described in this paper.

S–VIII. Detailed summary of the standard operating procedure for $DCFH_2$ preparation

The step-by-step SOP for the preparation of $DCFH_2$ from $DCFH_2$-DA by alkaline hydrolysis and liquid 2-phase extraction is described below.

PURPOSE AND USES OF THE PROBE

$DCFH_2$ (2',7'-dichlorodihydrofluorescein) is a water-soluble redox-sensitive fluorogenic probe. $DCFH_2$ is non-fluorescent in native state but becomes highly fluorescent following oxidation by oxidants such as reactive oxygen and nitrogen species (ROS/RNS), redox-active transition metals (e.g., Fe^{2+}), and activated peroxidases. Because $DCFH_2$ reacts with many different oxidants it cannot be employed as a ROS/RNS-selective probe. The probe can be used to detect the formation of oxidants in cell-free assays and cell-based systems. In cell-based systems, $DCFH_2$ may be used in addition to $DCFH_2$-DA

or in conjunction with $DCFH_2$-DA to discern between extracellular and intracellular oxidant production or to determine total intracellular and extracellular oxidant production, respectively.

IMPORTANT NOTES

- $DCFH_2$-DA (2',7'-dichlorodihydrofluorescein diactetate) is the starting compound.
- $DCFH_2$ (2',7'-dichlorodihydrofluorescein, molecular weight = 403.21 g/mol) is the end product.
- $DCFH_2$ is highly susceptible to oxidation upon light exposure. Prevent light exposure.
- $DCFH_2$ is susceptible to oxidation in an oxygen-rich environment. Samples should be stored under an atmosphere of inert gas, such as nitrogen gas.
- Keep the samples cooled to a maximum extent.
- $DCFH_2$ yield is approximately 54% and the final product is ≥ 95% pure.
- For the determination of $DCFH_2$ concentration by spectrophotometry, switch on the spectrophotometer 30 min before measurements to ensure stable output from the light bulb.
- For the determination of $DCFH_2$ concentration by spectrophotometry, use quartz cuvettes. Regular plastic cuvettes do not transmit deep UV light.
- Spectrofluorometric redox assays with $DCFH_2$ in a cuvette should be performed at a maximum DCF concentration of ~30 µM (i.e., oxidation end product) to prevent matrix effects. These matrix effects account for a plateau in fluorescence intensity at a DCF concentration of ≥ 30 µM and may skew read-out and interpretation of data.

MATERIALS AND EQUIPMENT

- $DCFH_2$-DA (CAS number 4091-99-0, molecular weight = 487.29 g/mol)
- sodium hydroxide (NaOH, CAS number 1310-73-2, molecular weight = 40.00 g/mol)
- hydrochloric acid (HCl, CAS number 7647-01-0, molecular weight = 36.46 g/mol)
- MilliQ
- chloroform (CAS number 67-66-3)
- methanol (CAS number 67-56-1)
- optional: dimethyl sulfoxide (DMSO, CAS number 67-68-5)
- Eppendorf tubes
- glass tubes (12 mL) with lids
- vortex mixer
- centrifuge with rotor buckets equipped to hold 12-mL glass tubes
- inert gas, such as nitrogen
- tin foil
- spectrophotometer
- quartz cuvette
- 1000- and 200-µL pipettes

PREPARATION OF $DCFH_2$

Preparation of $DCFH_2$-DA stock solutions

A. Dissolve $DCFH_2$-DA in methanol (MeOH) up to a concentration of 50 mM.
B. Prepare 100-µL aliquots in Eppendorf tubes.
C. Store the $DCFH_2$-DA stock solutions at -20 °C or -80 °C under a nitrogen atmosphere.

Deacetylation of $DCFH_2$-DA into $DCFH_2$ by alkaline hydrolysis

For best results, perform all procedures in a dark room.
A. Thaw the $DCFH_2$-DA stock aliquot.
B. Prepare a 100-mM sodium hydroxide (NaOH) stock solution in MilliQ.
C. Add $DCFH_2$-DA to the 100-mM NaOH stock solution in a glass tube at a $DCFH_2$-DA:solvent ratio ≥ 1:24 (e.g., 100 µL $DCFH_2$-DA stock in 2.5 mL NaOH solution).
D. Vortex and incubate the mixture for 15 min in the dark at room temperature.

Isolation and purification of $DCFH_2$

A. Prepare a 200 mM HCl stock solution.
B. Gradually add an equal volume of 200 mM aqueous HCl (equal to the volume fraction of the 100 mM NaOH) under continuous gentle vortexing to precipitate $DCFH_2$.
C. Place the mixture on ice for 5 min to complete $DCFH_2$ precipitation.
D. Centrifuge the glass tube at 2,000 × g for 15 min at 4 °C to pellet the precipitates; cover the tube in tin foil to prevent light exposure.
E. Aspirate the supernatant carefully using a pipette. Make sure a small layer of solvent remains to prevent exposure of $DCFH_2$ to room air.
F. Add 4 mL of ice-cold acidified MilliQ (pH = 1, from HCl).
G. Repeat steps C-E 2 more times to remove excess salt.
H. Equilibrate the sample to room temperature in the dark.
I. Add 4 mL of chloroform under continuous gentle vortexing to extract $DCFH_2$ from the aqueous phase.
J. Remove the aqueous phase (supernatant) with a pipette. Make sure that all aqueous solvent is removed.
K. Evaporate the chloroform under a continuous stream of nitrogen gas at room temperature. Cover the tube with tin foil to shield the sample from light if this step cannot be performed in a dark room.
L. Dissolve the $DCFH_2$ pellet in methanol or DMSO to a desired concentration up to 100 mM, taking into account the starting amount of $DCFH_2$-DA, a yield of approximately 54%, and a final $DCFH_2$ assay concentration of < 100 µM, depending on the application.
M. Aliquot the stocks when desired, purge with nitrogen gas, and store at -20 °C or -80 °C in the dark.

Determination of $DCFH_2$ concentration

A. Thaw the $DCFH_2$ stock at room temperature in the dark.
B. Dilute the prepared $DCFH_2$ stock in methanol to a concentration between 10 and 130 µM. For $DCFH_2$ in DMSO stocks, make sure that the final fraction of DMSO is ≤ 1% to prevent interference by DMSO absorption. The 130-µM $DCFH_2$ concentration corresponds to an optical density (absorption) of 1.0. Spectrophotometric measurements at an optical density of > 1.0 are unreliable.
C. Record the absorption of the sample at 287 nm in a quartz cuvette. Ensure that the measurements are zeroed to blank (methanol only or with an equivalent fraction of DMSO).
D. Calculate the $DCFH_2$ concentration with the following formula:

(1) $c = A / (\varepsilon \cdot l)$

A = optical density at 287 nm (i.e., the absorption value) (unitless)
ε = molar extinction coefficient of $DCFH_2$ in methanol (in $L \cdot mol^{-1} \cdot cm^{-1}$) = $7.6 \cdot 10^3$ $L \cdot mol^{-1} \cdot cm^{-1}$
c = concentration (in $mol \cdot L^{-1}$)
l = path length through the cuvette (in cm), typically 1 cm

S–IX. Determination of $DCFH_2$ molar extinction coefficient

The molar extinction coefficient (ε) can be used to determine the $DCFH_2$ concentration in $DCFH_2$ stock solutions.

Materials and methods: Desiccated $DCFH_2$ samples that that contained ≥ 3 mg of $DCFH_2$ (n = 5) were redissolved in MeOH and diluted to a 40-µM concentration. Absorption was measured and the molar extinction coefficient (λ = 287 nm) was calculated according to the Beer-Lambert law[9]. Sample fluorescence (λ_{ex} = 513 ± 5 nm and λ_{em} = 523–700 ± 5 nm) was determined directly thereafter, in which the area under the curve of the fluorescence emission spectrum was subsequently compared to that of a 40-nM DCF reference sample, corresponding to 0.1% $DCFH_2$ auto-oxidation.

Results: The mean ± SEM molar extinction coefficient of $DCFH_2$ in MeOH at λ = 287 nm was calculated to be $7.6 \pm 1.5 \cdot 10^3$ $M^{-1} \cdot cm^{-1}$ in samples containing < 0.001% DCF.

Conclusion: For the spectrophotometric determination of $DCFH_2$ concentration in MeOH, a molar extinction coefficient of $7.6 \cdot 10^3\ M^{-1} \cdot cm^{-1}$ and a wavelength of 287 nm should be used. It should be noted that the spectroscopic determination of $DCFH_2$ concentration directly in DMSO is unreliable because deep UV spectra at < 300 nm in this solvent are inaccurate. The $DCFH_2$ concentration of DMSO stock solutions can be determined in methanol granted that the fraction of DMSO does not exceed 1%.

S–X. Solvent- and pH-dependent changes in $DCFH_2$ spectral properties

The spectral properties of a chromophore may change in a solvent- and pH-dependent manner. Solvent- and pH-dependent changes in spectral properties may affect experimental outcomes in various ways and therefore warrant examination.

Materials and methods: The absorption spectra of $DCFH_2$ (40 µM, λ = 200–400 nm) were obtained in MeOH, MilliQ, and HEPES buffer (10 mM HEPES, 150 mM NaCl, pH = 6 or 12).

Results: The ground state absorption spectra of $DCFH_2$ in MeOH, MilliQ, and HEPES buffer (pH = 6) exhibited a uniform absorption peak at λ = 287 nm (Figure S8A, B, and C, respectively), albeit the peak amplitude differed in a solvent- and pH-dependent manner. The absorption spectrum in MilliQ entailed a deep UV peak at λ = 209 nm (Figure S8B, inset), which is in good correspondence to previously reported spectral data on $DCFH_2$[1]. The shape of the red absorption bands differed per solvent, confirming solvent-induced effects on the ground state absorption spectra. More importantly, $DCFH_2$ absorption was pH-dependent in buffered aqueous solution (Figure S8C), characterized by a bathochromic shift from λ_{max} = 287 nm at pH = 6 to λ_{max} = 305 nm at pH = 12. The pH-dependence is in agreement with literature[1].

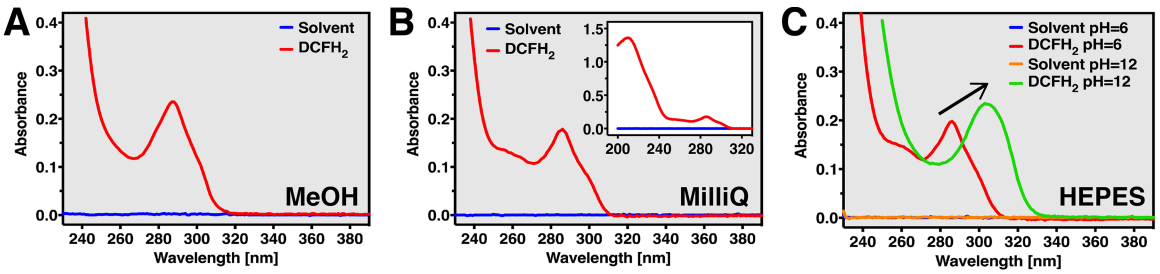

Figure S8. Solvent- and pH-dependent ground state absorption spectra of $DCFH_2$ in MeOH (Panel A), MilliQ (Panel B), and HEPES buffer (Panel C; pH = 6 and 12).

Conclusions: The ground state absorption spectra of $DCFH_2$ are solvent- and pH-dependent. These properties should be taken into account when conducting absorption-based assays, such as spectroscopic quantification of $DCFH_2$ content in cell lysates.

S–XI. Stability of $DCFH_2$-DA and $DCFH_2$ in organic solvents

The stability of dissolved redox-sensitive fluoregenic probes is vital to assay quality and post-preparation shelf life. The stability of $DCFH_2$-DA and $DCFH_2$ were therefore determined in the two most commonly used solvents under standard storage conditions.

Materials and methods: The stability of $DCFH_2$ in MeOH and DMSO was determined and compared to that of $DCFH_2$-DA, which has good long-term stability in non-aqueous organic solvents. Freshly prepared $DCFH_2$ (in MeOH) and $DCFH_2$-DA (in DMSO) stocks were diluted (20 µM final concentration) into both solvents, aliquoted, purged with N_2 gas, and stored at -20 °C in the dark for 0–28 d. Formation of DCF as a measure of the degree of auto-oxidation was determined spectrofluorometrically (λ_{ex} = 513 ± 5 nm and λ_{em} = 523-650 ± 5 nm, n = 3/time point) as a function of storage time. The area under the curve (AUC) of the fluorescence emission spectra was calculated and plotted as a percentage relative to the AUC of a 20-µM DCF reference sample, which was freshly

prepared and measured at each individual time point, to correct for differences in excitation light intensity over time.

Results: The stability of $DCFH_2$ and $DCFH_2$-DA was assessed in MeOH (Figure S9A) and DMSO (Figure S9B), indicating that both compounds were stable over a period of 28 d when stored at -20 °C in the dark.

Moreover, although longer-term stability was not formally tested, stock solutions of $DCFH_2$ in MeOH that were stored for more than one year have been successfully used without signs of auto-oxidation or $DCFH_2$ degradation (i.e., no decrease in DCF fluorescence intensity under standardized experimental redox conditions)[10,11].

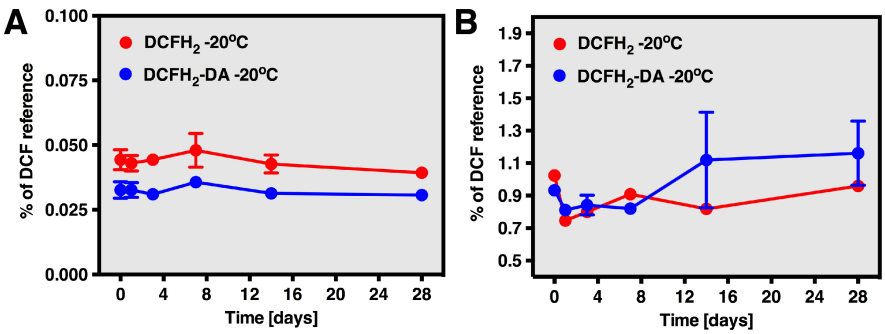

Figure S9. Long-term stability of $DCFH_2$-DA and $DCFH_2$ in MeOH (Panel A) and DMSO (Panel B) stored at -20 °C in the dark.

Conclusion: $DCFH_2$-DA and $DCFH_2$ are stable for at least a month when stored at -20 °C in the dark.

PART 2: USE OF $DCFH_2$ IN CELL-FREE ASSAYS

S–XII. Spectrofluorometric $DCFH_2$ oxidation assays in cell-free systems

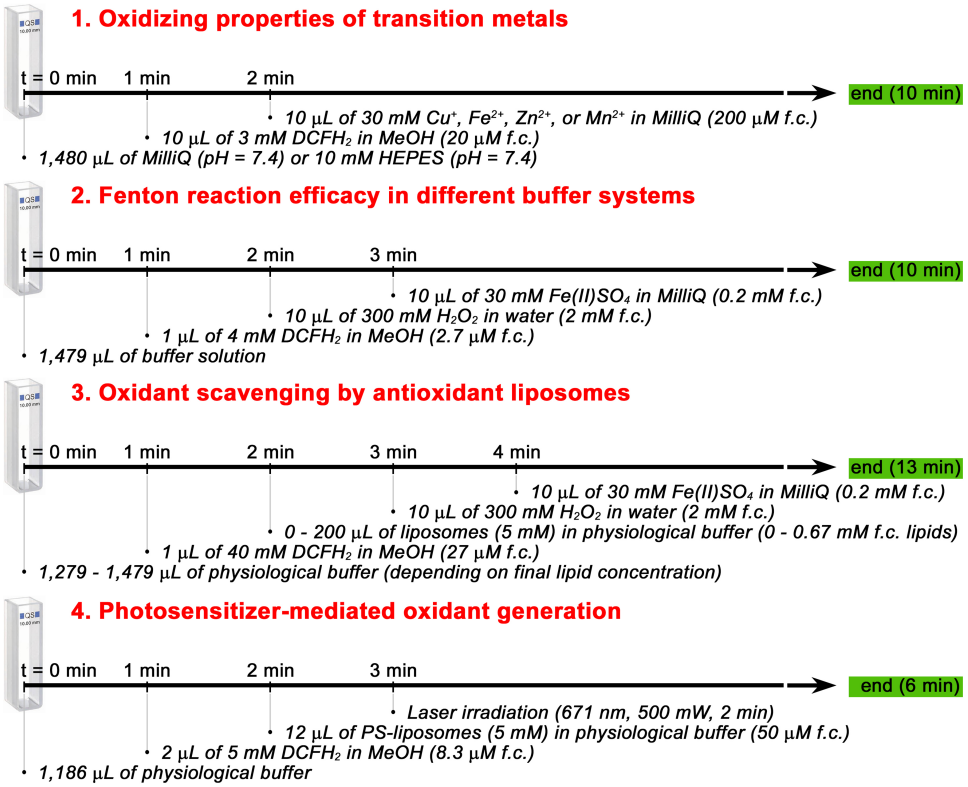

Figure S10. Summary of test arms where $DCFH_2$ oxidation was spectrofluorometrically determined in cell-free systems. f.c.: final concentration; PS: photosensitizer.

The experimental setup consisted of four different scenarios that are summarized in Figure S10. The $DCFH_2$ → DCF conversion was measured spectrofluorometrically at λ_{ex} = 500 ± 5 nm and λ_{em} = 523 ± 5 nm in kinetics mode during continuous stirring and Peltier-maintained temperature (Cary Eclipse, Varian).

Oxidizing properties of transition metals (TMs)

Materials and methods: The oxidizing potential of monovalent and divalent cationic TMs (Cu^+, Fe^{2+}, Zn^{2+}, and Mn^{2+}, all from Cl^- salt) to catalyze $DCFH_2$ oxidation in the presence of O_2 was analyzed spectrofluorometrically in time-based acquisition mode (λ_{ex} = 500 ± 5 and λ_{em} = 523 ± 5 nm, t = 6 min) using $DCFH_2$ (20 µM). A cuvette was loaded with solvent, to which $DCFH_2$ and TM ions or solvent control (ethanol for Fe^{2+}, Zn^{2+}, and Mn^{2+} or 2.5 M NaCl in MilliQ for Cu^+) were added at 1 and 2 min, respectively. All data were normalized to baseline fluorescence by subtracting the mean fluorescence emission from t = 0–55 s from all data points per sample.

Results: The reactivity of TMs towards $DCFH_2$ was determined in MilliQ (pH = 7.4) over time. A considerable increase in DCF fluorescence occurred following the addition of Cu^+ to the reaction medium containing $DCFH_2$. In contrast, marginal-to-no DCF formation occurred following the addition of Mn^{2+} or Zn^2. The reaction between $DCFH_2$ and Fe^{2+} led to a decrease in DCF fluorescence. This effect is most likely the result of $DCFH_2$ (over)oxidation into non-fluorescent end products by the highly reactive Fe^{2+} in the absence of competing substrates for oxidation (e.g., HEPES; Figure 2A).

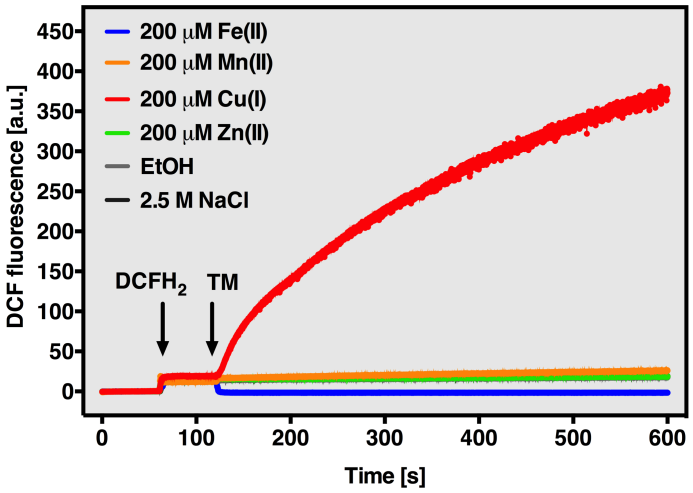

Figure S11. Reaction kinetics of TMs and solvent controls (ethanol (EtOH) for Fe^{2+}, Mn^{2+}, and Zn^{2+} and 2.5 M NaCl for Cu^+) in the presence of $DCFH_2$. Assays were conducted in MilliQ according to scheme 1 in Figure S10. The concentrations listed in the legends refer to final concentration in the cuvette.

Fenton reaction efficacy in different buffer systems

The oxidizing efficacy of the Fenton reaction ($Fe^{2+} + H_2O_2$ → $Fe^{3+} + {\bullet}OH + OH^-$) was determined in a variety of buffer systems.

Materials and methods: $DCFH_2$ (27 µM), H_2O_2 (2 mM), and Fe^{2+} (200 µM from $Fe(II)SO_4$) were added at t = 1, 2, and 3 min, respectively, to a cuvette loaded with Tris (50 mM Tris, 150 mM NaCl), sodium bicarbonate (30 mM, $NaHCO_3$, 30 mM NH_4Cl), HEPES (10 mM HEPES, 150 mM NaCl), phosphate-buffered saline (PBS; 7 mM Na_2HPO_4, 3 mM NaH_2PO_4, 130 mM NaCl), or citrate-phosphate (100 mM sodium citrate, 200 mM Na_2HPO_4) buffer (all pH = 7.4). The reactions were monitored spectrofluorometrically in kinetics mode. All data were normalized to baseline fluorescence by subtracting the mean fluorescence emission from t = 0–55 s from all data points per sample.

Oxidant scavenging by antioxidant liposomes

The ability of liposomes containing several types of antioxidants to attenuate Fenton reaction-mediated conversion of $DCFH_2$ to DCF was assessed.

Materials and methods: Antioxidant liposomes composed of DSPC and DSPE-PEG_{2000} were prepared in physiological buffer (10 mM HEPES, 150 mM NaCl, pH = 7.4, 0.293 osmol/kg) at a 96:4 molar ratio according to[12] using the lipid film hydration technique. The liposomes contained 0.1 µmol γ-tocopherol, 0.1 µmol α-tocopherol, 0.25 µmol curcumin, 0.5 µmol melatonin, and 0.1 µmol α-lipoic acid per mL of physiological buffer (Table S1). The liposomes were neither sized nor subjected to size exclusion chromatography following hydration and stored at 4 °C under a nitrogen atmosphere in the dark. Due to the instability of some of the components in aqueous solvent[13] the liposomes were used within 2 d after preparation. A cuvette was loaded with physiological buffer, to which $DCFH_2$ (27 µM), liposome solution (0.00–0.67 mM lipid), H_2O_2 (300 mM), and Fe^{2+} (30 mM from $FeSO_4$) were added at t = 1, 2, 3, and 4 min, respectively.

Photosensitizer-mediated oxidant generation

$DCFH_2$ was used to determine the oxidant-generating potential of liposomes encapsulating the hydrophobic photosensitizers (PS) zinc phthalocyanine and aluminum phtalocyanine (ZnPC and AlPC, respectively).

Materials and methods: PS-encasulating liposomes were prepared in physiological buffer from DPPC and DSPE-PEG_{2000} (96:4 molar ratio, 5 mM lipid, 0.003 PS:lipid ratio) as described in[11]. Their oxidizing potential during irradiation with a continuous wave solid state diode laser light (λ = 671 nm, CNI Laser, Changchun, China) was assessed spectrofluorometrically in kinetics mode. $DCFH_2$ (2 µL 5 mM stock; 8 µM final concentration) and liposomes (12 µL 5 mM lipid stock, 50 µM final lipid and 0.15 µM PS concentration) were added to a cuvette containing physiological buffer at t = 1 and 2 min, respectively. The sample was irradiated with 500-mW laser light during t = 3–5 min to induce PS-mediated oxidant generation as described in[11].

PART 3: USE OF $DCFH_2$ IN CELL-BASED ASSAYS

S–XIII. Platelet isolation and sample preparation

Materials and methods: Blood from healthy volunteers (MJR and MH) was collected via an open system[12] into a citrate solution (1:9 ratio, 129 mM trisodium citrate) and centrifuged (200 × g, 10 min, RT) to prepare platelet-rich plasma (PRP). The PRP was aspirated, 100 nM prostaglandin E_1 (PGE_1) was added, and the platelets were pelleted by centrifugation (280 × g, 15 min, RT). Next, the supernatant was discarded and the pellet was gently reconstituted in 5 mL of 0.2-µm filtered wash buffer (138 mM NaCl, 5 mM KCl, 34 µM Na_2HPO_4, 44 µM KH_2PO_4, 42 µM $NaHCO_3$, 5 mM trisodium citrate, 2.5 mM citric acid, 6 mM D(+)-glucose, 100 nM PGE_1, pH = 7.4). The platelet count was determined on an automated cell counter at the Laboratory of Clinical Chemistry of the Academic Medical Center.

The platelets were subsequently pelleted (280 × g, 15 min, RT), reconstituted to a concentration of 100 × 10^6 platelets/mL in 0.2-µm filtered assay buffer (138 mM NaCl, 5 mM KCl, 34 µM Na_2HPO_4, 44 µM KH_2PO_4, 42 µM $NaHCO_3$, 10 mM HEPES, 6 mM D(+)-glucose, 1 mM $MgCl_2$, 100 nM PGE_1, pH = 7.4) and loaded into a 96-well plate. Next, convulxin (250 ng/mL), human thrombin (0.2 U/mL), PMA (0.5 µM), or the respective solvent controls were added. Lastly, samples were incubated with $DCFH_2$ (50 µM) for 20 min at RT, after which the fluorescence was read in a microplate reader (λ_{ex} = 460 ± 40 and λ_{em} = 520 ± 20 nm, n = 6/group).

S–XIV. Cell culture and DNA quantification for $DCFH_2$ oxidation assays

RAW 264.7 cells, a murine macrophage cell line, and 3T3 cells, a murine fibroblast cell line, were cultured in Dulbecco's modified Eagle medium (DMEM) supplemented with 10% FBS, 100 U/mL penicillin, 100 µg/mL streptomycin, and 2 mM L-glutamine under standard culture conditions (a humidified atmosphere of 5% CO_2 and 95% air at 37 °C). Cells were subcultured every 3–4 days at a 1:5 ratio following detachment by gentle scraping (RAW 264.7 cells) or at a 1:10 ratio following trypsinization (10 min at 37 °C) in a 2:1:1 accutase:accumax:PBS mixture (3T3 cells). For experimental assays, the cells were harvested, seeded in 24-wells plates, and grown to 80% confluence (RAW 264.7 cells) or 100% confluence (3T3 cells).

To determine the total DNA content per well, cells were lysed in 750 µL (RAW 264.7 cells) or 1,000 µL of 0.2 M NaOH in MilliQ for 1 h at 37 °C, after which 10 µL of cells lysate was mixed with 200 µL of 0.01 µg/mL Hoechst 33342 in phosphate buffer (35 mM Na_2HPO_4, 15 mM NaH_2PO_4, 2 M NaCl, pH = 7.4). The DNA content per well was subsequently determined spectrofluorometrically (λ_{ex} = 340 ± 40 and λ_{em} = 460 ± 40 nm) against a fish sperm DNA standard curve (0–250 µg/mL, dissolved in 0.2 M NaOH in MilliQ).

S–XV. Detection of intracellular and extracellular oxidant formation in fibroblasts and stimulated macrophages

$DCFH_2$ and $DCFH_2$-DA may be employed simultaneously for the detection of intra- and extracellularly produced oxidants. This approach was tested using murine 3T3 fibroblasts subjected to anoxia and reoxygenation as well as murine RAW 264.7 macrophages stimulated with various ROS/RNS-inducing compounds.

Extracellular localization of $DCFH_2$

Materials and methods: oxidant production was induced in RAW 264.7 and 3T3 cells incubated with $DCFH_2$ or $DCFH_2$-DA, after which intracellular DCF fluorescence was assayed by flow cytometry to determine $DCFH_2$(-DA) uptake.

3T3 cells were incubated under hypoxic conditions for 4 h in serum-free medium in a custom-built culture chamber (saturated with 95% N_2 and 5% CO_2 at 37 °C)[14], which results in mitochondrial superoxide anion ($O_2^{\bullet-}$) formation upon reoxygenation. Control cells were maintained under normoxic culture conditions (95% air and 5% CO_2 at 37 °C) for 4 h. The cells were harvested, washed twice in PBS, and resuspended in serum-free medium (1×10^6 cells/mL). DCF fluorescence was measured by flow cytometry following 30-min incubation (37 °C) with $DCFH_2$ or $DCFH_2$-DA (50 µM). Ten thousand events were collected in the gated region (viable cells; high FSC/SSC ratio). The mean DCF fluorescence per event (λ_{ex} = 488 nm and λ_{em} = 530 ± 30 nm, n = 12/group) was calculated and served as a measure of intracellular $DCFH_2 \rightarrow$ DCF conversion.

RAW 264.7 cells were harvested, washed in 5 mL PBS (500 × g, 5 min, RT), and resuspended in 12 mL serum-free medium (1×10^6 cells/mL). The cell suspension was aliquoted into 3-mL samples that were incubated with $DCFH_2$-DA (50 µM), $DCFH_2$ (50 µM), or solvent control (DMSO, 1% vol/vol) for 30 min at 37 °C. Next, the cells were washed twice in PBS, resuspended in serum-free medium (1×10^6 cells/mL), and incubated with phorbol 12-myristate 13-acetate (PMA; 2 µM) for 20 min at 37 °C to activate the membrane-bound $O_2^{\bullet-}$-generating enzyme NADPH oxidase-2 (NOX2)[15]. DCF fluorescence was measured by flow cytometry as described above.

Detection of extracellular and intracellular redox reactions

Materials and methods: RAW 264.7 and 3T3 cells were incubated with $DCFH_2$-DA or $DCFH_2$ (50 µM) in PBS, during which DCF fluorescence was measured in a fluorescence plate reader set to kinetics mode (λ_{ex} = 460 ± 40 and λ_{em} = 520 ± 20 nm, t = 20 min at 2-min intervals, 37 °C). A cell-free plate containing $DCFH_2$-DA or $DCFH_2$ (50 µM) in PBS was read separately to adjust for $DCFH_2$-DA or $DCFH_2$ auto-oxidation, respectively, in the incubation medium. The mean DCF fluorescence (from $DCFH_2$ or $DCFH_2$-DA) of the second, cell-free plate was subtracted from each tested sample at the corresponding time point. The adjusted data were corrected for differences in baseline fluorescence by subtracting the data at t = 0 min from each subsequent time point per sample. Lastly, the corrected

fluorescence data were normalized to total DNA content per well (S–XIV) to adjust for differential cell seeding density.

Cell stimulation assays

Materials and methods: 3T3 cells were incubated for 4 h in serum-free medium under hypoxic conditions (95% N_2 and 5% CO_2, 37 °C) and compared to untreated (normoxic) controls (n = 6/group). RAW 264.7 cells were stimulated with interferon gamma (IFN-γ; 50 U/mL, 16 h pretreatment), which induces •NO generation through iNOS activation[16], and/or phorbol 12-myristate 13-acetate (PMA; 2 µM in the assay incubation medium), which elicits NADPH oxidase-2 (NOX2)-dependent extracellular $O_2^{\bullet-}$ generation at the plasma membrane (n = 6/group)[17].

To investigate the specific contribution of each stimulant to the observed redox alterations in RAW 264.7 macrophages, the effects of IFN-γ (induces nitric oxide (•NO) formation, which can be detected as extracellular NO_2^-) or PMA (induces $O_2^{\bullet-}$ formation) were blocked by addition of *N*ω-nitro-L-arginine methyl ester hydrochloride (L-NAME) or diphenyliodonium (DPI), respectively. Extracellular nitrite (NO_2^-) was determined in culture medium using a colorimetric kit (Griess Reagent System, Promega, Madison, WI) according to the manufacturer's instructions. The data were plotted as mean ± SD (n = 12/group) and tested using one-way ANOVA and Tukey's multiple comparisons test. The level of statistical significance was set at $p < 0.05$.

The effects of L-NAME (1 mM; 16 h pretreatment), DPI (2.5 µM; 1 h pretreatment), or solvent controls (activated group) on RAW 264.7 cells stimulated with IFN-γ (50 U/mL; 16 h pretreatment) and PMA (2 µM) were further investigated using $DCFH_2$ (50 µM) and compared with untreated controls (resting group). The data were plotted as mean ± SD and the mean corrected DCF fluorescence at t = 20 min was tested using one-way ANOVA and Tukey's multiple comparisons test. The level of statistical significance was set at $p < 0.05$.

Results: Pretreatment of RAW 264.7 macrophages with IFN-γ (+IFN; 50 U/mL) for 16 h led to significant •NO formation, measured as extracellular NO_2^-, compared to the untreated cells (-IFN; $p < 0.001$; Figure S12). Co-incubation with the nitric oxide synthase inhibitor L-NAME (1 mM) led to a significant reduction in •NO formation compared to IFN-γ-stimulated cells ($p < 0.001$), but remained significantly higher relative to untreated cells ($p < 0.001$).

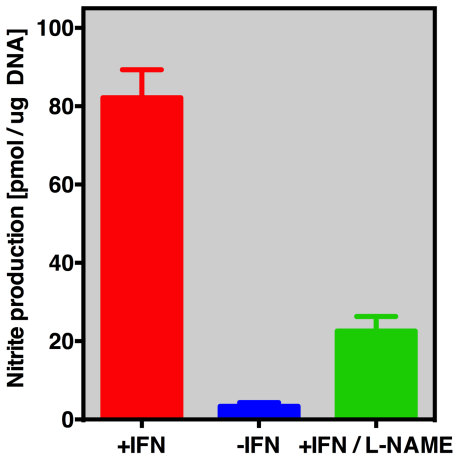

Figure S12. Nitrite production by RAW 264.7 macrophages, which reflects intracellular •NO generation, following stimulation with IFN-γ (positive control, red), in the absence of IFN-γ (negative control, blue), and under stimulatory conditions in the presence of the •NO-specific scavenger L-NAME (green).

Inhibition of iNOS or NOX2 induction through co-incubation with L-NAME or DPI, respectively, resulted in a significant reduction in exctracellular oxidant formation compared to the activated group ($p < 0.001$) under both conditions (Figure S13).

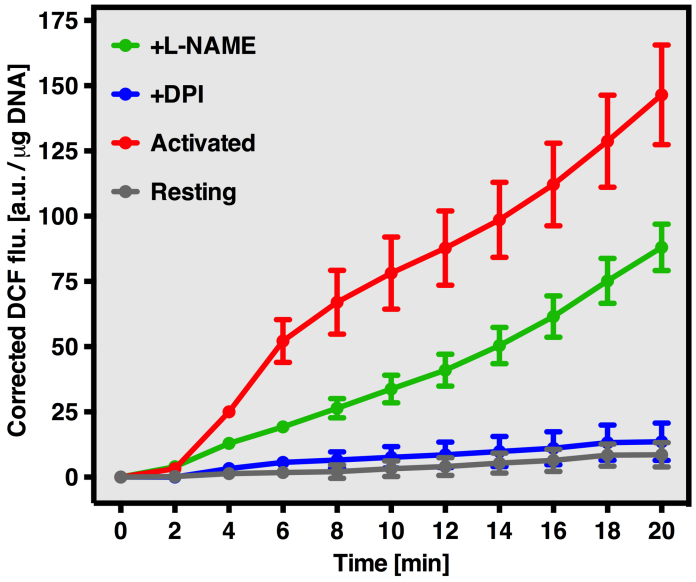

Figure S13. Extracellular oxidant production by RAW 264.7 macrophages in resting state (control, gray) or activated by the •NO inducer IFN-γ and the $O_2^{\bullet-}$ inducer PMA (positive control, red), also in the presence of the $O_2^{\bullet-}$ scavenger DPI (blue) and the •NO scavenger L-NAME (green).

PART 4: PREPARATION AND IN VITRO VALIDATION OF LIPOSOMES FOR HEPATOTARGETING

S–XVI. Preparation of hepatotargeted liposomes

Materials and methods: All liposomal formulations for hepatotargeting liposomes were composed of varying molar fractions of DPPC, cholesterol, and the galactose-bearing ganglioside GM1 (GM1) and/or lactosyl phosphatidyl ethanolamine (LPE). Fluorescently labeled liposomes were prepared by incorporating 5 mol% NBD-PC at the expense of DPPC.

Liposomes were prepared by the lipid film hydration technique according to[18]. Lipids were mixed at the desired concentration and ratios, after which the organic solvent was evaporated under a steam of nitrogen gas. The lipid film was vacuum exsiccated for at least 30 min and hydrated with physiological buffer. Next, the sample was sonicated with a tip sonicator until the solution turned clear, generally within 3–5 min.

For the *in vitro* hepatocyte uptake and all *in vivo* experiments, liposome size was adjusted by sequential extrusion through a 100- and 50-nm polycarbonate filter (Whatman, Maidstone, UK; 11× per filter) using a hand-operated extrusion device (Mini Extruder, Avanti Polar Lipids, Alabaster, AL). Liposome size and polydispersity index were assessed by photon correlation spectroscopy (Zetasizer 3000, Malvern Instruments, Malvern, PA) according to[11]. Data on all formulations used in this substudy are listed in Table S2. Final phospholipid concentration of all lipid and liposome stocks was determined according to[19].

Table S2. Composition, size, and polydispersity of hepatotargeted liposomes.

Experiment	Molar ratio DPPC : chol : LPE : GM1 : NBD-PC	Size [mean ± SD nm]	Polydispersity [mean ± SD]
Cholesterol optimization *In vitro*, HepG2 (uptake/toxicity assay; S–XVIII, S–XIX)	85 : 0 : 5 : 5 : 5	141.7 ± 3.0	0.371 ± 0.014
	75 : 10 : 5 : 5 : 5	145.7 ± 1.3	0.116 ± 0.052
	65 : 20 : 5 : 5 : 5	195.6 ± 3.8	0.157 ± 0.026
	55 : 30 : 5 : 5 : 5	171.1 ± 2.5	0.127 ± 0.009
	45 : 40 : 5 : 5 : 5	145.4 ± 0.8	0.215 ± 0.028
GM1 optimization *In vitro*, HepG2 (uptake/toxicity assay; S–XVIII, S–XIX)	52.5 : 40 : 0 : 2.5 : 5	163.0 ± ND	0.118 ± 0.015
	50 : 40 : 0 : 5 : 5	165.6 ± 1.3	0.162 ± 0.041
	47.5 : 40 : 0 : 7.5 : 5	180.3 ± 1.3	0.372 ± 0.019
LPE optimization *In vitro*, HepG2 (uptake/toxicity assay; S–XVIII, S–XIX)	47.5 : 40 : 2.5 : 5 : 5	144.6 ± 1.0	0.217 ± 0.016
	45 : 40 : 5 : 5 : 5	144.0 ± 1.8	0.203 ± 0.002
	42.5 : 40 : 7.5 : 5 : 5	149.0 ± 2.0	0.348 ± 0.065
	45 : 40 : 2.5 : 2.5 : 5	151.2 ± ND	0.355 ± 0.066
In vitro, mouse hepatocytes (uptake assay; S–XVIII)	47.5 : 40 : 2.5 : 5 : 5	89.2 ± 0.4	0.039 ± 0.008
In vivo, whole liver uptake; S–XXI	50 : 40 : 0 : 5 : 5	86.0 ± 1.6	0.088 ± 0.125
	47.5 : 40 : 2.5 : 5 : 5	93.9 ± 2.6	0.051 ± 0.051
In vivo, intrahepatic distribution; S–XXII	50 : 40 : 0 : 5 : 5	91.8 ± 0.9	0.040 ± 0.022
	47.5 : 40 : 2.5 : 5 : 5	101.2 ± 1.1	0.019 ± 0.013
In vivo, oxidative stress during IR; ; S–XXIII	55 : 40 : 0 : 5 : 0	84.2 ± 1.1	0.029 ± 0.016

S–XVII. HepG2 and hepatocyte culture

Materials and methods: Human hepatocellular carcinoma (HepG2) cells were cultured in William's E (WE) medium supplemented with 10% (vol/vol) FBS, 100 U/mL penicillin, 0.1 mg/mL streptomycin, 2 mM L-glutamine, 5 µg/mL insulin, and 50 µM hydrocortisone under standard culture conditions. Cells were subcultured every 3–4 days in a 1:5 subculture ratio following detachment by trypsinization (15 min at 37 °C) in a 2:1:1 accutase:accumax:PBS mixture. For liposome uptake assays, the cells were harvested, seeded into 24-well plates, and grown to 100% confluence.

Primary mouse hepatocytes were isolated as described below (S–XXII), with the exception that the hepatocyte fraction was reconstituted in culture medium directly after the first round of centrifugation. The cells were subsequently counted with a hemocytometer (BLAUBRAND counting chamber, BRAND, Wertheim, Germany) and seeded into 24-well plates at 90% confluence. The cells were used within 24 h after seeding.

S–XVIII. *In vitro* uptake of hepatotargeted liposomes

Materials and methods: HepG2 cells were cultured as described in section S–XVII, seeded into 24-well plates, and grown to 100% confluence. Cells were rinsed once with PBS (37 °C) and incubated with NBD-labeled liposomes mixed with phenol red-free unsupplemented medium (0, 0.5, 1, 1.5, 2, and 2.5 mM final lipid concentration; 5 mol% NBD-PC) for 30 min under standard culture conditions. The incubation medium was discarded and the cells were washed thrice in PBS (37 °C). NBD fluorescence was determined spectrofluorometrically as a measure for cellular uptake (λ_{ex} = 460 ± 40 and λ_{ex} = 520 ± 20 nm). Data were corrected for total DNA content per well as described in S–XIV.

Results: The uptake of liposomes with a generic composition of DPPC:chol:LPE:GM1:NBD-PC (Table S2) by HepG2 cells is plotted as function of cholesterol molar fraction (Figure S14A), GM1 molar fraction (Figure S14B), and LPE molar fraction (Figure S14C).

First, the cholesterol fraction was optimized using liposomes composed of 5 mol% GM1, LPE, and NBD-PC. Increasing fractions of cholesterol (0–40 mol%) were incorporated at the expense of DPPC. Liposome uptake was lipid concentration-dependent and increased with rising cholesterol content (Figure S14A). This effect was likely attributable to the increase in membrane rigidity at higher cholesterol content[20], an effect that has been reported to improve the uptake of galactosylated liposomes by HepG2 cells as well as primary mouse hepatocytes[21]. Hence, a 40-mol% cholesterol fraction was used in all subsequent experiments.

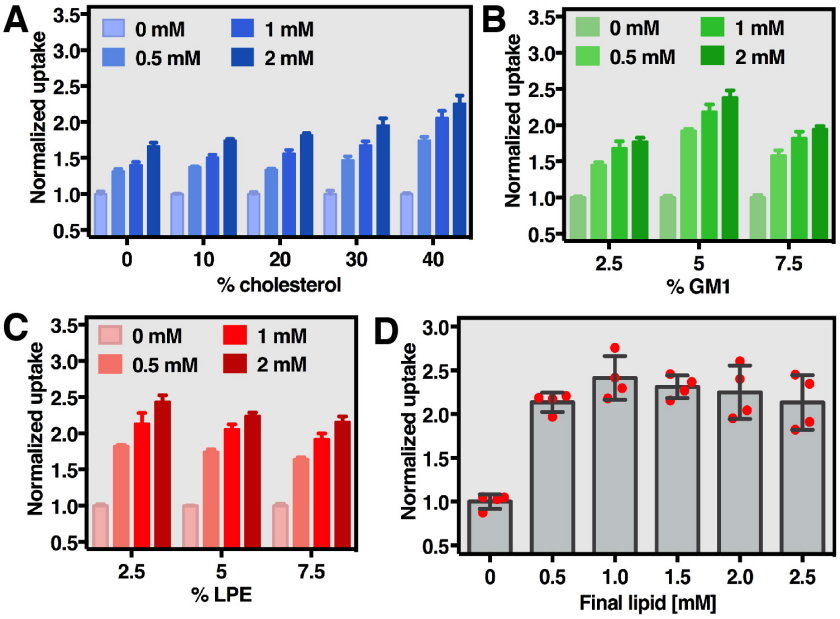

Figure S14. Uptake of hepatotargeted liposomes by cultured hepatocytes. Panels A–C show data from HepG2 cells that were incubated with fluorescently-labeled liposomes (0, 0.5, 1, and 2 mM final lipid concentration) containing increasing molar fractions of cholesterol (Panel A), GM1 (Panel B), and LPE (Panel C). The formulations are specified in Table S2. Cellular fluorescence, which was used as a measure of liposome uptake, was corrected for total DNA content per well and normalized to control (i.e., 0 mM lipid). Data represent mean ± SD for n = 4. Panel D shows data from primary mouse hepatocytes that were incubated with increasing concentration of liposomes (0-2.5 mM final lipid concentration) containing 5 mol% GM1 + 2.5 mol% LPE. Cellular fluorescence was corrected for total DNA content per well and normalized to controls (i.e., 0 mM lipid). Data represent mean ± SD for n = 4.

Next, liposomal GM1 content was optimized because incorporation of this ligand not only allows for galactose-mediated targeting, but also provides a steric barrier that is critical for preventing uptake of liposomes by Kupffer cells (KCs) during *in vivo* experiments in mice[22]. The essence of steric hindrance in hepatotargeting was further demonstrated by the improved parenchymal/non-parenchymal cell uptake ratio found with galactosylated liposomes (conjugated to N-glutaryl-phosphatidyl ethanolamine) following steric stabilization with PEG[23]. Accordingly, cellular uptake of liposomes composed of cholesterol (40 mol%), NBD-PC (5 mol%), and increasing fractions of GM1 (2.5, 5, and 7.5 mol%) at the expense of DPPC was analyzed (Figure S14B). Maximum uptake was achieved with liposomes containing a 5% molar fraction of GM1, which is in agreement with previous work in mice showing maximal uptake of galactosylated liposomes containing 5 mol% of cholesterol-complexed galactose[24].

The addition of a second galactose moiety (LPE) was investigated using liposomes composed of GM1 (5 mol%), cholesterol (40 mol%), and NBD (5 mol%). LPE was included at increasing fractions (2.5, 5, and 5 mol%) at the expense of DPPC. Maximum uptake was observed with liposomes containing 2.5 mol% LPE (Figure S14C). Considering that the optimal galactose density for hepatocyte uptake is generally does not exceed 5 mol%[24], an additional formulation composed of 2.5 mol% GM1 and 2.5 mol% LPE was tested. Uptake of these liposomes was not superior to that of DPPC:chol:GM1:NBD-PC (50:40:5:5) and DPPC:chol:LPE:GM1:NBD-PC (50:40:2.5:5:5) liposomes

(data not shown). These formulations are referred to as GM1 and GM1 + LPE liposomes, respectively, from here onward.

To determine the optimal lipid concentration for the in vivo uptake experiments, fluorescently-labeled GM1 + LPE liposomes were sized to < 100 nm and incubated with primary mouse hepatocytes at increasing final lipid concentrations (Figure S14D). An increase in fluorescence was seen up to 1.0-mM final lipid concentration ($p < 0.05$ compared to 0 mM), which was consequently chosen as the plasma final lipid concentration in the *in vivo* uptake experiments (S-XXI and -XXII).

S–XIX. In vitro cytotoxicity of hepatotargeted liposomes

Materials and methods: To determine liposome cytotoxicity, cells were cultured and seeded in 24-well plates as described in S–XVII. Liposomes containing 5 mol% NBD-PC (Table S2) were added to cells at a 0-, 0.5-, 1-, 1.5-, 2-, and 2.5-mM final lipid concentration in phenol red-free unsupplemented WE medium.

After 30-min incubation at standard culture conditions, cell viability was assessed by measuring mitochondrial redox activity with water-soluble tetrazolium-1 (WST-1) as described in[11]. WST-1 is reduced to a formazan chromophore by metabolically active cells and hence serves as an indirect measure of mitochondrial activity[25]. Absorption was recorded at 450 nm. Data were corrected for total DNA content per well as described in S–XIV and normalized to the 0-mM control group.

Results: No statistically significant reduction in WST-1 conversion was seen for any of the formulations (Figure S15), indicating that all formulations were non-toxic to cultured HepG2 cells up to a final lipid concentration of 2.5 mM. Consequently, the GM1 and GM1 + LPE liposomes were used in the *in vivo* uptake experiments.

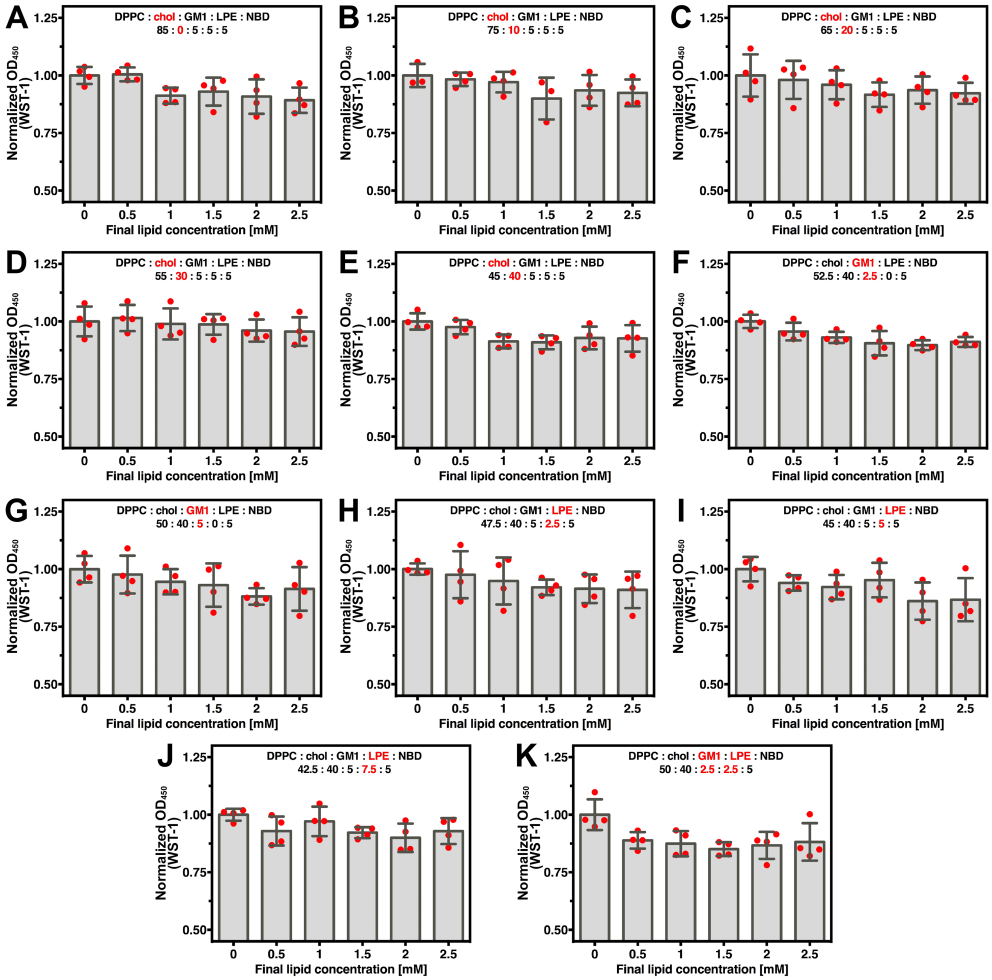

Figure S15. Liposome cytotoxicity in HepG2 cells. Cytotoxicity was analyzed using the WST-1 assay following 30-min incubation with liposomes at increasing final lipid concentrations (0-2.5 mM). Panels A–K show the

concentration-dependent cytotoxicity (as normalized OD_{450}) data for all tested formulations. The formulations are specified in each frame, in which the change in the molar fraction of a specific lipid bilayer component is indicated in red. Data represent mean ± SD for n = 4.

PART 5: INTRAVITAL MEASUREMENT OF OXIDATIVE STRESS IN MOUSE LIVERS WITH HEPATOTARGETED LIPOSOMES

S–XX. Animal care and anesthesia

Materials and methods: The study was approved by the animal ethics committee of the Academic Medical Center at the University of Amsterdam (BEX103177). All animals were treated in accordance with the Guide for the Care and Use of Laboratory Animals (NIH publication 85–23, rev. 2011) and institutional guidelines. Male C57BL/6J mice (n = 50, 25–30 g, 8–12 wk old, Charles River, Saint-Germain-sur-l'Arbresle, France) were acclimated for 1 wk under standardized laboratory conditions in a temperature- and humidity-controlled cabinet (21–23 °C, 45–65% humidity) with a 12-h light/dark cycle and *ad libitum* access to water and standard chow (Rat and Mouse No. 1 Maintenance Diet, Special Diet Services, Essex, UK).

All animals received Temgesic (0.06 mg/kg buprenorphine subcutaneously) as analgesia prior to induction of general anesthesia, which was induced and maintained with isoflurane (2.0–2.5% in 1:1 O_2:air at 1 L/min) through a nasal cap. Body temperature was measured rectally and maintained at 37 °C throughout the experiment by means of a heating lamp and a customized heating stage.

S–XXI. Intrahepatic liposome accumulation

Materials and methods: Intrahepatic liposome accumulation was investigated by intravital microscopy and spectroscopy. Mice were anesthetized as described in S–XX and secured onto a heating platform (37 °C). The left medial lobe was exteriorized following a midline laparotomy, positioned onto a custom-build supra-abdominal stage, flushed with 0.9% NaCl solution, and covered with saran wrap to prevent tissue desiccation over de course of intravital imaging and spectroscopy[26].

The microscopy setup, depicted in Figure S16, consisted of a custom-modified stereo fluorescence microscope (model M165 FC, Leica Microsystems, Wetzlar, Germany) equipped with a Peltier-cooled DFC420C camera, a Planapo 1.0 × objective lens, a 0.5 × video objective (C-mount), a time-based acquisition module, filter sets for brightfield (420 nm cut on filter) and fluorescence (λ_{ex} = 470 ± 20 nm, λ_{em} = 515 nm long pass) microscopy, and a Leica EL6000 light source. The C-mount adapter was modified at the Department of Medical Innovation and Development to house a spectroscopy component. The C-mount adapter was cut directly above the lens such that a light separation module was placed between the microscope aperture and the camera. The module contained an interference filter that was positioned at an angle relative to the incident light, causing ~1% of light to be diverged orthogonally into an optical fiber connected to a spectrometer (model QE65000, Ocean Optics, Dunedin, FL) while ~99% of light was transmitted onto the camera's CCD chip. This allowed concomitant microscopy and spectroscopy.

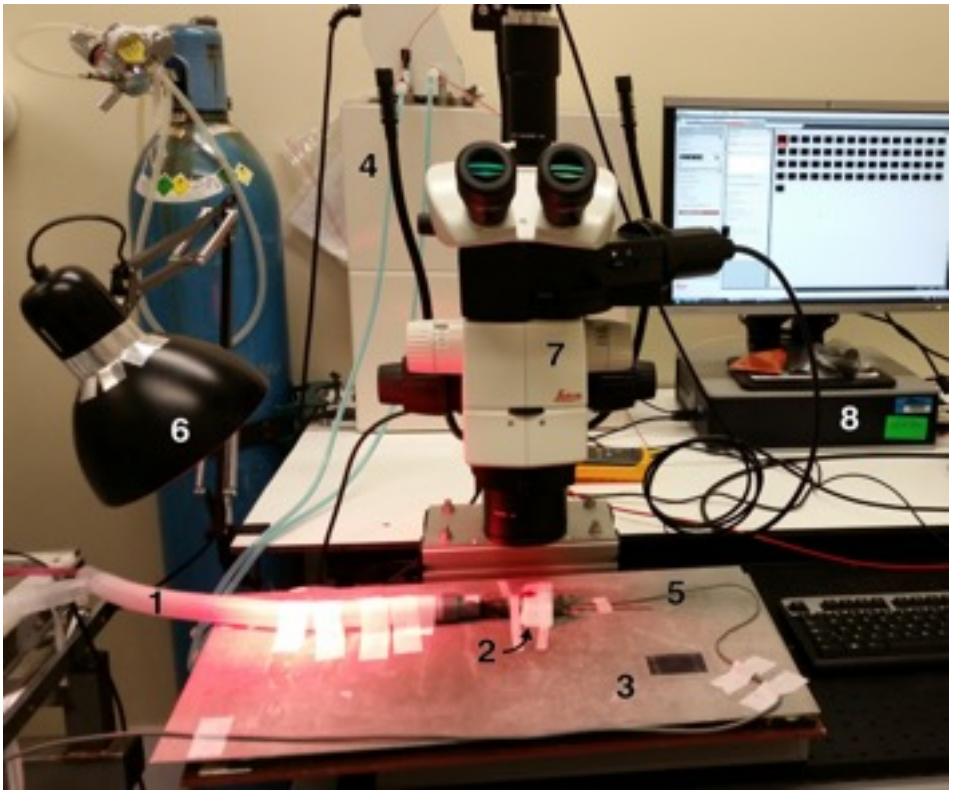

Figure S16. Intravital microscopy setup. Animal anesthesia was induced in an induction chamber and maintained through a nasal cap (1). The animals (2) were placed on a bespoke heating stage (3) connected to a temperature controller (4). Core body temperature of the animals, measured with an anal temperature probe connected to the anesthesia machine (5), was further regulated with a red light-emitting heating lamp (6). The microscopy setup (7) consisted of a custom-modified stereo fluorescence microscope equipped with a Peltier-cooled DFC420C color camera and a Leica EL6000 light source. The C-mount adapter was modified at the Department of Medical Innovation and Development to house a spectroscopy interface placed between the microscope aperture and the camera. The module contained an interference filter that was positioned at an angle relative to the incident light, causing ~1% of light to be diverged orthogonally into an optical fiber connected to a spectrometer while ~99% of light was transmitted onto the camera's CCD chip without interfering with image quality. This allowed concomitant microscopy and spectroscopy, controlled via a PC workstation (8).

After the animal was positioned under the microscope, time-based image acquisition was started (t = 120 min at 2-min intervals). The spectroscopy component was not used during these experiments. The camera exposure time was 150.8 ms with 4.0 × gain and 1.89 × optical zoom. Automated shutter control of the excitation light source was engaged to ensure 1-ms illumination for excitation and subsequent closing of the shutter to prevent fluorophore bleaching between measurements. Directly after acquisition of the first image, NBD-labeled GM1 and GM1 + LPE liposomes (5 mol% NBD; 0.06 µmol lipid/g body weight in 200 µL physiological buffer) were injected through the penile vein. The liposomes were prepared as described in S–XVI.

NBD fluorescence was analyzed as a measure of whole-liver uptake using ImageJ software (National Institutes of Health, Bethesda, MD). Images were converted to 8-bit greyscale, after which total pixel intensity was determined per time point and normalized to t = 0 min.

Animals were sacrificed by cardiac puncture and exsanguination directly after imaging. The liver, spleen, lungs, heart, stomach, intestine, kidney, bladder, and whole blood (from the heart) were extracted and snap-frozen in liquid nitrogen and stored at -80 °C until further analysis (S–XXIII).

Results: A rapid increase in tissue fluorescence was seen for both formulations within the first 40 min following liposomes administration (Figure S17). NBD fluorescence intensity thereafter gradually declined, possibly due to liposome degradation and biliary excretion of NBD. The latter was based on the observation of yellow-stained stools during internal organ removal following sacrifice. Liposomes containing GM1 + LPE accumulated more rapidly than those containing GM1 alone (t_{max} = 35 and 25 min, respectively), but the overall uptake of the GM1 formulation was greater. The optimal circulation times seen here correlate well to those reported in literature on galactose-labeled hepatotargeted liposomes, which show maximal liver uptake at ~30 min of circulation[21,24,27-29].

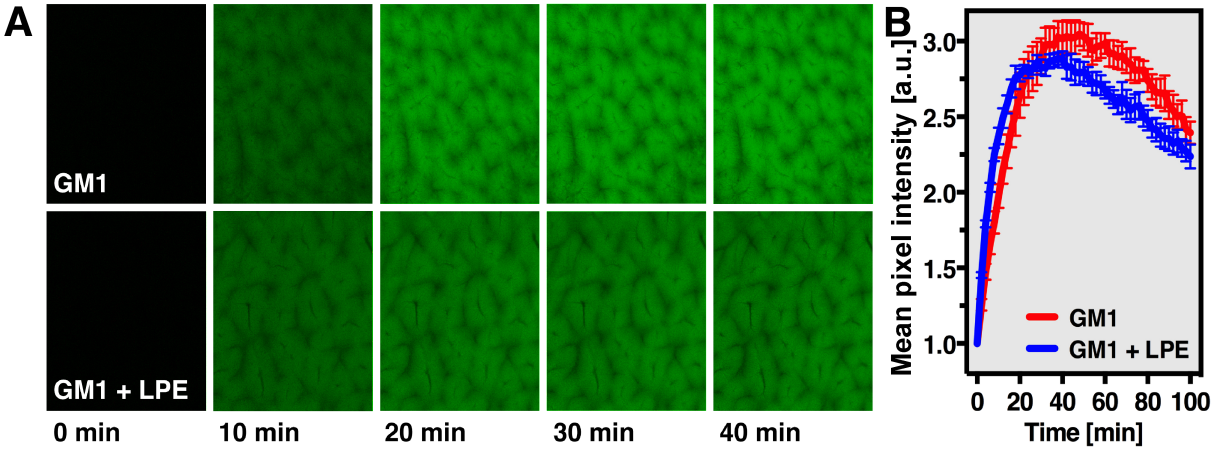

Figure S17. Hepatic uptake of GM1 and GM1 + LPE liposomes. Panel A shows hepatic NBD fluorescence as a measure for the total liver uptake of GM1 (top row) and GM1 + LPE liposomes (bottom row) was visualized using *in vivo* fluorescence microscopy. Panel B depicts total hepatic liposome uptake as a function of time. Therefore, fluorescence emission intensity was quantified by determining the total pixel intensity per frame, which was subsequently normalized to t = 0 min and plotted as a function of time after liposome infusion. Data represent mean ± SEM for n = 5.

S–XXII. Intrahepatic liposome distribution to parenchymal and non-parenchymal cells

Materials and methods: Fluorescently labeled GM1 and GM1 + LPE liposomes (5 mol% NBD, 0.06 µmol lipid/g body weight in 200 µL physiological buffer) were prepared as described in S–XVI, injected via the penile vein, and circulated for 25 or 35 min depending on whether liposomes contained GM1 + LPE or GM1, respectively. Animals in the control group received 200 µL of physiological buffer as vehicle control.

Before the end of the circulation time, a median laparotomy with transversal extension was performed and the liver was mobilized. Following injection and 5-min circulation of 100 IU heparin, the portal vein was cannulated with the tip of a 22-G intravenous cannula (Venflon, BD Biosciencies, Franklin Lakes, NJ) and the liver was perfused with sterile-filtered (0.2 µm) flush buffer (128 mM NaCl, 2.7 mM KCl, 10 mM HEPES, 0.67 mM Na_2HPO_4, 11 mM D+-glucose, pH = 7.4) for 5 min (n = 5/group). Next, the suprahepatic vena cava was cut to allow for optimal perfusate drainage and the liver was excised under continuous perfusion with flush buffer. The organ was placed on a heated petri dish (37 °C), transferred to a laminal flow cabinet, and perfused with sterile-filtered collagenase buffer (flush buffer with 5 mM $CaCl_2$, 5% bovine serum albumin (BSA), 0.02% collagenase IV, and 0.004% hyaluronidase, pH = 7.4) for 18 min (Figure S18). The tissue was gently homogenized using a cell strainer in collagenase buffer mixed with cell culture medium and sequentially extruded through a 100-, 70-, and 40-µm strainer (EASYstrainer, Greiner Bio-One, Kremsmünster, Austria) to generate single-cell suspensions. The mixture was subsequently divided into a hepatocellular- and non-parenchymal cell fraction by two rounds of centrifugation (50 × g, 5 min, 4 °C). While the pelleted hepatocytes were kept on ice, the non-parenchymal cell-containing supernatant was separated form cellular debris by two additional rounds of centrifugation (200 × g, 5 min, 4 °C). Both fractions were reconstituted in 5 mL cell culture medium and cells were counted using a hemocytometer. Cells were pelleted (200 × g, 5 min, 4 °C) and reconstituted in sterile-filtered FACS buffer (5% BSA in PBS) at a concentration of 10×10^6 cells/mL.

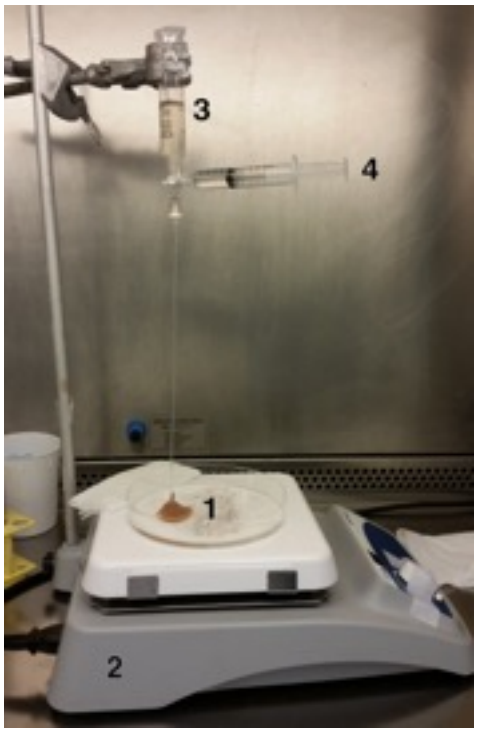

Figure S18. Perfusion setup. Following excision, the liver was placed in a sterile petri dish (1) onto a heating platform (2) in a laminar flow cabinet. The liver was perfused with collagenase buffer (3) through the main portal vein, which was cannulated with a 21-G cannula connected to a perfusion setup consisting of an open syringe holding the perfusion solution (3) and a second closed syringe connected via three-way tap (4) that was used to remove air from the system prior to perfusion.

Both fractions were incubated with fluorescently labeled anti-mouse F/80 (Brilliant Violet) and anti-mouse CD146 antibodies (APC; 100 ng antibody/1 × 10^6 cells in 100 µL FACS buffer) to stain Kupffer cells and endothelial cells, respectively, for 30 min at 4 °C in the dark. Samples were washed twice in 1 mL FACS buffer (600 × g, 5 min, 4 °C), resuspended in 1.5 mL ice-cold fixation buffer (0.5% paraformaldehyde in PBS), pelleted (600 × g, 5 min, 4 °C), and reconstituted in ice-cold FACS buffer for storage.

All samples were stored at 4 °C in the dark and analyzed within one week by flow cytometry (LSRFortessa, BD Biosciences, Franklin Lakes, NJ). Fluorescence was measured at $\lambda_{ex/em}$ = 405/450 nm (Brilliant Violet), $\lambda_{ex/em}$ = 488/530 nm (NBD), and $\lambda_{ex/em}$ = 640/675 nm (APC). Hepatocytes were gated based on their morphological characteristics (i.e., high FSC and SSC). KCs and endothelial cells from the non-parenchymal fraction were gated based on their fluorescence emission pattern, i.e., high Brilliant Violet/low APC and high APC/low Brilliant Violet fluorescence, respectively.

Twenty thousand events were collected in the gated region. Data were analyzed using FlowJo software (TreeStar Software, Ashland, OR) and expressed as mean NBD fluorescence/count. The hepatocyte/KC uptake ratio was calculated from paired hepatocyte and KC samples (i.e., from the same animal).

S–XXIII. Total body distribution of liposome uptake

Materials and methods: Tissue samples form liver, spleen, heart, stomach, intestine, kidney, bladder, and blood (400 µL) were transferred into ceramic bead-containing homogenizer tubes (MagNA Lyser Green Beads, Roche, Basel, Switzerland) containing 400 or 500 µL PBS, depending on the sample size. Samples were homogenized (6,500 rpm, 60 s, RT) using a MagNA Lyser tissue homogenizer (Roche). Thereafter, homogenates were diluted 50, 100, or 500 times in protein lysis buffer (0.2 M NaOH and 1% TX-100 in MilliQ) and total protein content was determined using a commercial kit (Pierce BCA Protein Assay Kit, Thermo Fisher, Waltham, MA). Tissue homogenates were transferred into 1.5-mL Eppendorf tubes and centrifuged (20,000 × g, 5 min, RT). Next, 150 µL of the supernatant was aspirated and transferred into glass tubes to which 500 µL $CHCl_3$ was added to extract NBC-PC

from the sample. Sample NBD content was subsequently quantified in the $CHCl_3$ fraction using fluorescence spectroscopy (λ_{ex} = 470 ± 10 and λ_{em} = 490–700 ± 10 nm). Emission spectra of each sample were integrated, corrected for dilution, and normalized to protein content (in µg/µL).

Results: Both GM1 and GM1 + LPE liposomes mostly accumulated in spleen, lung, and liver; all of which are part of the mononuclear phagocyte system[30]. Although NBD levels were greater in spleen and lung samples, this effect only emerged following correction of sample NBD levels for total protein content, which was approximately 8 and 26 x higher in liver and blood, respectively (data not shown). In addition, a trend towards more pronounced liposome uptake was observed for GM1 compared to GM1 + LPE liposomes in all organs including the liver, which is in accordance with the data presented in Figure S17.

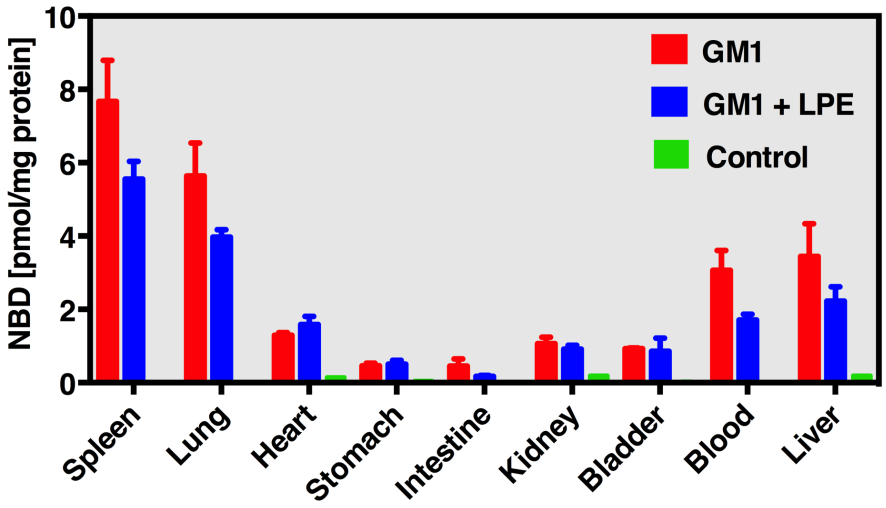

Figure S 19. Total body distribution of liposomes. Uptake of NBD-labeled hepatotargeted GM1 (red bars) and GM1 + LPE liposomes (blue bars; in pmol NBD/mg protein) was analyzed for different organs and compared to solvent controls (green bars). Data are plotted as mean ± SEM.

Conclusion: NBD-labeled hepatotargeted GM1 and GM1 + LPE liposomes mostly accumulated in organs that are part of the mononuclear phagocyte system. A trend towards more pronounced liposome uptake was noted for GM1 compared to GM1 + LPE liposomes.

S–XXIV. Real-time visualization of hepatocellular oxidative stress during ischemia/reperfusion with hepatotargeted liposomal $CDCFH_2$

Materials and methods: The redox-sensitive fluorogenic dye 5(6)-carboxy-$DCFH_2$ ($CDCFH_2$) was encapsulated into GM1 liposomes, the optimal formulation for *in vivo* hepatotargeting (Figure S17), with the aim of selectively visualizing hepatocellular oxidative stress during IR. $CDCFH_2$ was prepared from 5(6)-carboxy-$DCFH_2$-DA as described in S–VIII. GM1 liposomes were prepared and characterized as described in S–XVI, with the exception that the lipid film was hydrated with 260 µM $CDCFH_2$ (from 26 mM in DMSO, 1% DMSO) in physiological buffer. Unencapsulated probe was subsequently removed by size exclusion chromatography according to[12].

Induction of anesthesia and preparation of the median liver lobe were performed as described S–XX and S–XXI, respectively. In addition, the falciform ligament was dissected and a silicone sling functioning as a tourniquet was placed around the portal pedicle. A sling instead of a microvascular clamp was used in order to perform the entire surgical procedure under the intravital microscopy setup. Following positioning under the microscope, liposomes (0.1 µmol lipid/g body weight in 200 µL physiological buffer) were injected via the penile vein and circulated for 35 min. Next, ischemia was induced by clamping the portal pedicle for 60 min. At 30 min of ischemia, a brightfield image was taken to check for parenchymal blanching (a hallmark sign for ischemia[26]), and animals that did not show blanching were excluded. Sham animals underwent the exact same procedure with the exception that the sling was not tightened.

During reperfusion, CDCF fluorescence (resulting from oxidative stress-induced $CDCFH_2$ oxidation) was visualized by fluorescence microscopy and spectroscopy as described in S–XXI. All data were obtained in time-based acquisition (20 min at 2-min intervals). Images were acquired at a 298.5-ms exposure time with 4.0 × gain and 2.30 × optical zoom. For spectroscopy, spectra obtained at a 500-ms interval (with dark current correction) were integrated over the complete spectral width (i.e., λ = 250–1050 nm).

S–XXVI. Statistical analysis

Statistical analysis of all data (including the main text) was performed in GraphPad Prism 6 (GraphPad Software, La Jolla, CA). Data were analyzed using the unpaired Student's t-test or one-way ANOVA with Bonferroni correction. A p-value < 0.05 was considered statistically significant. Graphs show mean ± SEM unless stated otherwise in the figure legend or text.

References

(1) Wrona, M. and Wardman, P. *Free Radic Biol Med.* **2006**, *41*, 657-667.
(2) Mchedlov-Petrossyan, N. O.; Rubtsov, M. I.; and Lukatskaya, L. L. *Dyes Pigm.* **1992**, *18*, 179-198.
(3) Afri, M.; Frimer, A. A.; and Cohen, Y. *Chem Phys Lipids.* **2004**, *131*, 123-133.
(4) Spry, D. B.; Goun, A.; and Fayer, M. D. *J Phys Chem A.* **2007**, *111*, 230-237.
(5) Leonhardt, H.; Gordon, L.; and Livingston, R. *J Phys Chem.* **1971**, *75*, 245-249.
(6) Qian, S. Y. and Buettner, G. R. *Free Radic Biol Med.* **1999**, *26*, 1447-1456.
(7) Kalyanaraman, B.; Darley-Usmar, V.; Davies, K. J. A.; Dennery, P. A.; Forman, H. J.; Grisham, M. B.; Mann, G. E.; Moore, K.; Roberts, L. J.; and Ischiropoulos, H. *Free Radic Biol Med.* **2011**, *52*, 1-6**.**
(8) Martins, F. G.; Andrade, J. F.; Pimenta, A. C.; Lourenço, L. M.; Castro, J. R. M.; and Balbo, V. R. *Eclética Química.* **2005**, *30*, 63-71.
(9) Poggendorff, J. C. *Annalen der Physik,* J.A. Barth; 1852.
(10) Kloek, J.; Marechal, X.; Roelofsen, J.; Houtkooper, R.; van Kuilenburg, A.; Kulik, W.; Bezemer, R.; Neviere, R.; Vangulik, T.; and Heger, M. *Antioxid Redox Signal.* **2012**, *17*, 1109-1123**.**
(11) Broekgaarden, M.; de Kroon, A. I.; Gulik, T. M.; and Heger, M. *Curr Med Chem.* **2013**, *21*, 377-391.
(12) Heger, M.; Salles, I. I.; van Vuure, W.; Hamelers, I. H.; de Kroon, A. I.; Deckmyn, H.; and Beek, J. F. *Microvasc Res.* **2009**, *78*, 57-66.
(13) Heger, M.; van Golen, R. F.; Broekgaarden, M.; and Michel, M. C. *Pharmacol Rev.* **2014**, *66*, 222-307.
(14) Weijer, R.; Broekgaarden, M.; Krekorian, M.; Alles, L. K.; van Wijk, A. C.; Mackaaij, C.; Verheij, J.; van der Wal, A. C.; van Gulik, T. M.; Storm, G.; and Heger, M. *Oncotarget.* **2015**, *7*, 3341-3356**.**
(15) Bedard, K. and Krause, K. H. *Physiol Rev.* **2007**, *87*, 245-313.
(16) Xie, Q. W.; Whisnant, R.; and Nathan, C. *J Exp Med.* **1993**, *177*, 1779-1784.
(17) Griendling, K. K.; Sorescu, D.; and Ushio-Fukai, M. *Circ Res.* **2000**, *86*, 494-501.
(18) Torchilin, V. and Weissig, V. *Liposomes: a practical approach,* Oxford University Press; 2003.
(19) Rouser, G.; Fkeischer, S.; and Yamamoto, A. *Lipids.* **1970**, *5*, 494-496.
(20) Sułkowski, W. W.; Pentak, D.; Nowak, K.; and Sułkowska, A. *J Mol Struct.* **2005**, *744-747*, 737-747.
(21) Murao, A.; Nishikawa, M.; Managit, C.; Wong, J.; Kawakami, S.; Yamashita, F.; and Hashida, M. *Pharm Res.* **2002**, *19*, 1808-1814.
(22) Liu, D.; Liu, F.; and Song, Y. K. *Pharm Res.* **1995**, *12*, 508-512.
(23) Nag, A. and Ghosh, P. C. *J Drug Target.* **1999**, *6*, 427-438.
(24) Managit, C.; Kawakami, S.; Yamashita, F.; and Hashida, M. *J Pharm Sci.* **2005**, *94*, 2266-2275.
(25) Berridge, M. V.; Herst, P. M.; and Tan, A. S. *Biotechnol Ann Rev.* **2005**, *11*, 127-152.
(26) van Golen, R. F.; Reiniers, M. J.; Heger, M.; and Verheij, J. *J Hepatol.* **2015**, *62*, 975-977.
(27) Wang, S.N.; Deng, Y.H.; Xu, H.; Wu, H.B.; Qiu, Y.K.; and Chen, D.W. *Eur J Pharm Biopharm.* **2006**, *62*, 32-38.
(28) Yamauchi, H.; Kikuchi, H.; Sawada, M.; Tomikawa, M.; and Hirota, S. *J Microencapsul.* **1994**, *11*, 287-296.
(29) Kawakami, S.; Wong, J.; Sato, A.; Hattori, Y.; Yamashita, F.; and Hashida, M. *Biochim Biophys Acta.* **2000**, *1524*, 258-265.

(30) Van Furth, R.; Cohn, Z. A.; Hirsch, J. G.; Humphrey, J. H.; Spector, W. G.; and Langevoort, H. L. *Bull World Health Organ.* **1972**, *46*, 845-852.